

PLATINUM-GROUP MINERALS FROM FIVE PLACER DEPOSITS IN BRITISH COLUMBIA, CANADA

ANDREI Y. BARKOV[§] AND MICHAEL E. FLEET

Department of Earth Sciences, University of Western Ontario, London, Ontario N6A 5B7, Canada

GRAHAM T. NIXON[¶] AND VICTOR M. LEVSON

*British Columbia Geological Survey, Ministry of Energy, Mines and Petroleum Resources, PO Box 9320, Stn. Prov. Govt.,
Victoria, British Columbia V8W 9N3, Canada*

ABSTRACT

Platinum-group minerals (PGM) from a selected suite of gold- and platinum-group-element (PGE) placer deposits in British Columbia have been analyzed using the electron-microprobe (EMP). The PGM placer grains ($n = 70$, 0.1–1.5 mm in size) principally comprise various Pt–Fe–(Cu) alloys: “Pt₃Fe”-type alloys [Fe-rich platinum (formerly, ferroan platinum: Bayliss *et al.* 2005) or isoferroplatinum], Fe-rich Pt with an atomic Σ PGE:(Fe + Cu + Ni) ratio of 3.6–5.6, “(Pt,Ir)₂Fe”-type alloy, members of the tulameenite–tetraferroplatinum solid-solution series extending from Pt₂Fe(Cu,Ni) toward PGE_{1+x}(Fe,Cu,Ni)_{1-x}, less common Ir-dominant Ir–Os–(Ru–Pt) alloys, subordinate Os-dominant alloys, and minor Ru-rich alloys and rutheniridosmine, the latter with an atomic Ir:Os:Ru proportion close to 1:1:1. Trace amounts of PGE sulfides and sulfarsenides: cooperite PtS, Ni-rich cuproiridsite (Cu,Ni,Fe)(Ir,Rh,Pt)₂S₄, unusual sperrylite-type [(Pt,Rh,Fe)(As,S)_{2-x}] and platarsite-type [PtAs_{1-x}S_{1+x}, or unnamed Pt(S,As)_{2-x}] phases, and unnamed (Ir,Rh,Pt)S (?) crystallized at a late stage in low-S environments. Some PGM grains contain micro-inclusions of diopside, augite, ferro-edenite, a potassian sodic-calcic amphibole (richterite?), talc, clinocllore and euhedral quartz. High values of *mg#* [100Mg/(Mg + Fe)] of the ferromagnesian minerals in these inclusions suggest highly magnesian source-rocks. Textural and compositional data, in particular the zoned intergrowths of Pt–Fe–(Cu) alloy grains, which broadly resemble the zoned Pt–Pd–Cu stannides from the Noril’sk complex, indicate the following sequence of crystallization: (Pt,Ir,Rh)₃Fe → (Pt,Ir,Rh)_{1+x}(Fe,Cu)_{1-x} or Pt₂Fe(Cu,Ni). The zoned Pt–Fe–Cu alloys likely formed by fractional crystallization of primary solid-solutions under closed-system conditions as a result of increase in the activity of Cu in the residual liquid after an early-stage (magmatic) crystallization of the Cu-poor core. The Cu-rich Pt–Fe alloys formed around these core zones and at their peripheries during a significant drop in temperature at a late stage of crystallization of the composite alloy grains. The compositions of micro-inclusions and exsolution lamellae of Os- and Ir-dominant alloys in Pt–Fe alloys imply uniform temperatures of equilibration within the range 750–800°C. The compositions of Cu-rich Pt–Fe alloys, PGE sulfides and sulfarsenides, and exsolution lamellae of Os- and Ir-dominant alloys, observed in intimate association with Pt–Fe alloys, are likely related to the crystallization of the coexisting Pt–Fe alloys. Narrow zones of Pt–Fe alloys richer in Pt and poor in Fe, observed at the boundary of placer Pt–Fe alloy grains, provide evidence for a removal of Fe and corresponding addition of Pt as a result of interaction with a low-temperature fluid. The terrane affinities, compositions and associations of the placer PGM examined appear consistent with two types of potential source-rocks, associated with Alaskan-type intrusions and the Atlin ophiolite complex. The preservation of faceted morphologies on many of the placer PGM grains implies a relatively short distance of transport from their source.

Keywords: platinum-group elements, platinum-group minerals, Pt–Fe alloys, Pt–Fe–Cu alloys, zoning, Ir–Os alloys, Ir–Os–Ru alloys, PGE mineralization, placer deposits, Alaskan–Uralian-type complexes, ultramafic-mafic rocks, British Columbia, Canada.

SOMMAIRE

Nous avons analysé les minéraux du groupe du platine (MGP) d’une suite choisie de gisements placer d’or et d’éléments du groupe du platine (EGP) en Colombie-Britannique au moyen d’une microsonde électronique. Les grains des MGP des placers ($n = 70$, 0.1–1.5 mm de diamètre) sont faits d’une variété d’alliages Pt–Fe–(Cu): alliage de type “Pt₃Fe” (platine riche en fer ou isoferroplatinum), platine riche en fer avec un rapport atomique Σ PGE:(Fe + Cu + Ni) de 3.6 à 5.6, alliage de type “(Pt,Ir)₂Fe”,

[§] *Present address:* Department of Earth and Planetary Sciences, McGill University, 3450 University Street, Montreal, Quebec H3A 2A7, Canada. *E-mail address:* abarkov@eps.mcgill.ca

[¶] *E-mail address:* graham.nixon@gems8.gov.bc.ca

membres de la solution solide tulameenite-tétraferroplatinum allant de $Pt_2Fe(Cu,Ni)$ vers $PGE_{1+x}(Fe,Cu,Ni)_{1-x}$, et moins couramment, un alliage Ir–Os–(Ru–Pt) à dominance d'iridium, des alliages subordonnés à dominance d'Os, et une proportion mineure d'alliages riches en Ru et ruthéniridosmine, cette dernière avec une proportion Ir:Os:Ru voisine de 1:1:1. Des quantités en traces de sulfures et de sulfarséniures des EGP: cooperite PtS, cuproiridosite nickelifère $(Cu,Ni,Fe)(Ir,Rh,Pt)_2S_4$, des phases inhabituelles de type sperrylite $[(Pt,Rh,Fe)(As,S)_{2-x}]$ et platarsite $[PtAs_{1-x}S_{1+x}]$, ou $Pt(S,As)_{2-x}$ sans nom], ainsi que $(Ir,Rh,Pt)S$ (?) sans nom, ont cristallisé à un stade tardif dans un milieu relativement dépourvu en soufre. Certains des grains de MGP contiennent des micro-inclusions de diopside, augite, ferro-édenite, une amphibole sodi-calcique riche en potassium (richtérite?), talc, clinocllore et quartz idiomorphe. Des valeurs élevées de $mg\#$ $[100Mg/(Mg + Fe)]$ des minéraux ferromagnésiens inclus semblent indiquer une source fortement magnésienne. Les données texturales et compositionnelles, en particulier les intercroissances zonées des grains d'alliage Pt–Fe–(Cu), qui ressemblent *grosso modo* aux grains de stannures de Pt–Pd–Cu zonés du complexe de Noril'sk, indiquent la séquence de cristallisation $(Pt,Ir,Rh)_3Fe \rightarrow (Pt,Ir,Rh)_{1+x}(Fe,Cu)_{1-x}$ ou $Pt_2Fe(Cu,Ni)$. Les alliages Pt–Fe–Cu zonés se seraient formés par cristallisation fractionnée de solutions solides primaires en système fermé suite à une augmentation de l'activité du cuivre dans le liquide résiduel après un stade précoce qui a produit un noyau à faible teneur en Cu. Les alliages Pt–Fe riches en Cu se sont formés autour de ces noyaux au cours d'une chute importante de la température à un stade tardif de la cristallisation. Les compositions des micro-inclusions et des lamelles d'exsolution des alliages à dominance de Os et de Ir dans un hôte Pt–Fe implique des températures uniformes d'équilibre autour de 750–800°C. Les compositions des alliages cuprifères de Pt–Fe, des sulfures et des sulfarséniures des EGP, et les lamelles d'exsolution des alliages à dominance de Os et Ir étroitement associées aux alliages Pt–Fe, seraient liées à la cristallisation des alliages Pt–Fe coexistants. Les étroites zones d'alliages Pt–Fe plus riches en Pt et pauvres en Fe à la bordure des grains témoignent d'un lessivage de Fe et d'une addition correspondante de Pt suite à une interaction avec une phase fluide à faible température. Selon les affinités avec les socles, la composition et les associations des MGP des placers, il semble y avoir deux sortes de roches-mères, des massifs intrusifs de type Alaska et le complexe ophiolitique de Atlin. La préservation des cristaux idiomorphes dans plusieurs cas fait penser que ces minéraux seraient près de leurs sources.

(Traduit par la Rédaction)

Mots-clés: éléments du groupe du platine, minéraux du groupe du platine, alliages Pt–Fe, alliages Pt–Fe–Cu, zonation, alliages Ir–Os, alliages Ir–Os–Ru, minéralisation, placers, complexe de type Alaska–Ourales, roches ultramafiques-mafiques, Colombie-Britannique, Canada.

INTRODUCTION

Gold- and "platinum"-bearing placer deposits have been worked in British Columbia since they were first discovered in the mid- to late 1800s. Of the 106 platinum-group-element (PGE)-bearing mineral occurrences currently listed in the provincial MINFILE database, approximately half occur in placer deposits, and virtually none of these PGE occurrences have been traced to their bedrock source. An investigation of known and suspected Au–PGE-enriched placers in British Columbia was conducted recently by Levson *et al.* (2002) in order to evaluate relationships to their original lode-sources using sedimentological, geochemical and mineralogical criteria (*e.g.*, Raicevic & Cabri 1976, Nixon *et al.* 1990, Levson & Morison 1995, Knight *et al.* 1999a,b).

The present study provides detailed mineralogical descriptions and compositions of platinum-group minerals (PGM) at five of these PGE placer sites in British Columbia. Our objectives here are (1) to characterize the speciation, associations and textural relationships of various PGM from the Au–PGE placer deposits, (2) to document compositional variations observed in these PGM, (3) to establish the composition of micro-inclusions of various silicates and hydrous silicates derived from the mineralized host-rock(s) and

present in some of these PGM, (4) to make a comparison with PGM from other PGE deposits, (5) to suggest likely primary sources for these placer PGM grains and nuggets, and (6) to discuss some aspects of the crystallization history of these PGM.

SAMPLE DESCRIPTIONS AND GEOLOGICAL SETTING

The location of placer concentrates analyzed in this study are shown in Figure 1 in relation to the tectono-stratigraphic setting of occurrences of ultramafic rocks and serpentinite in British Columbia, which are potential source-rocks for the placer PGE mineralization. In addition, details of sample sites are provided in the Appendix.

Sample VLE 2001–12c

This placer concentrate sample (58 g) was collected from the O'Donnel River in the Atlin Mining District, approximately 32 km southeast of the community of Atlin and 20 km above Atlin Lake (Fig. 1). It consists of a black, moderately well-sorted medium sand, with some coarse sand and minor granules. Although comprised predominantly of mafic minerals, some felsic minerals were also noted. Substantial quantities of gold are present in the concentrate sample.

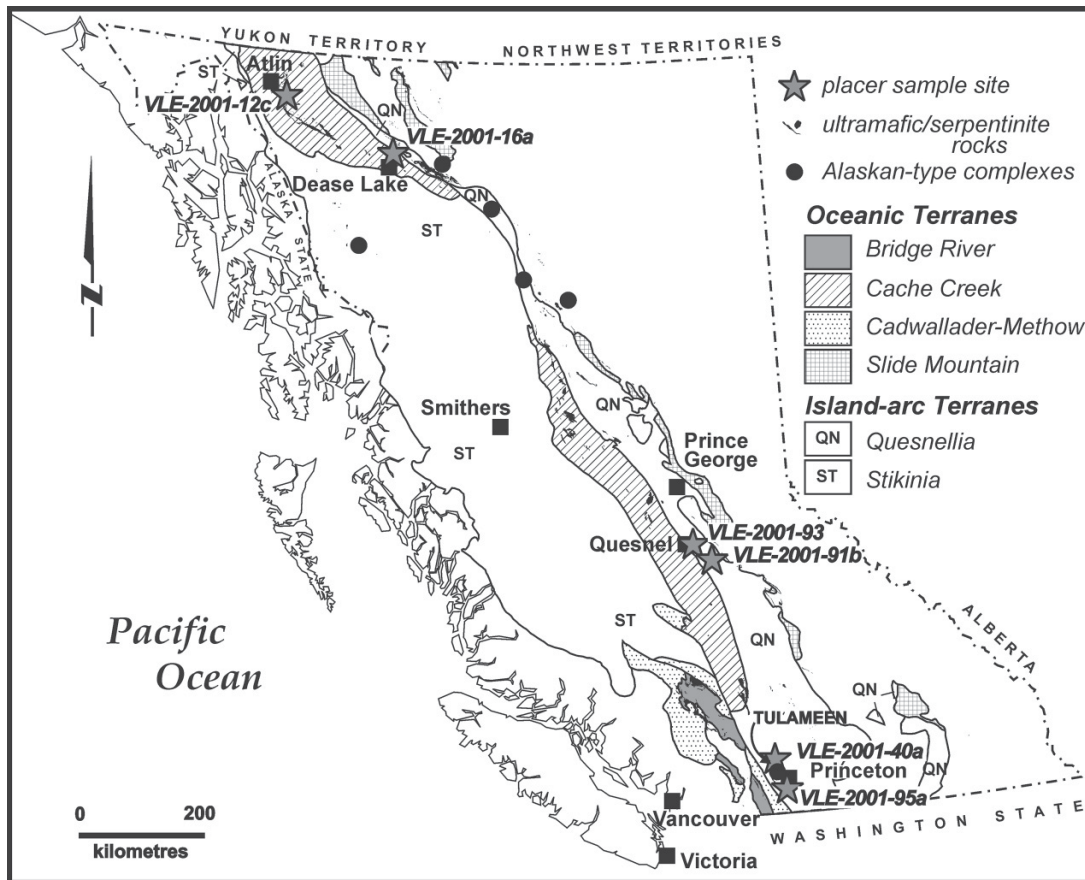


FIG. 1. Sample locations of PGM placer concentrates analyzed in this study and their tectonostratigraphic setting. Also shown are the distribution of potential source-rocks for the placer PGM: ultramafic rocks and serpentinite in oceanic (ophiolitic) terranes, and known occurrences of Alaskan-type ultramafic-mafic complexes (including Tulameen) in British Columbia.

Sample VLE 2001-16a

This sample (39 g) was recovered from Dease Creek, about 25 km northwest of Dease Lake townsite and 7 km upstream from where the creek enters Dease Lake. The concentrate comprises a black, well-sorted fine sand. Fine gold and possible PGM grains are visible in the sand. The concentrate was sluiced from gravels resting on bedrock at depths of about 1–2 m below the surface. The analyzed sample includes only the non-magnetic fraction, but magnetite is abundant in sluice concentrates from the site. Other minerals reported in the concentrates include abundant pyrite and hematite as well as Au–Ag alloy, platinum mineral(s), garnet and galena.

Sample VLE 2001-40a

This sample (18 g) was collected from Lockie Creek, approximately 1 km from its mouth at Otter Lake and 4 km north of Tulameen. The concentrate is a dark gray to black, well-sorted fine sand. Fine gold and possible PGM grains are visible in the sample. Magnetite, pyrite and rare chalcopyrite also are present.

Sample VLE 2001-93

This concentrate sample (205 g) is from the Quesnel River, approximately 3 km east of the town of Quesnel in the Cariboo Mining District. The analyzed sample is a light brown, moderately well-sorted fine sand. The concentrate has an unusually high concentration of felsic minerals as well as silt and clay. Some magnetite and visible gold grains are also present.

Sample VLE 2001–95a

This sample (140 g) is from the Similkameen River, about 15 km above its confluence with the Tulameen River near the town of Princeton. The sample comprises a black to dark brown, well-sorted, non-magnetic fine sand. The observed minerals include abundant mafic constituents, including olivine, garnet, pyrite and chalcopyrite.

SAMPLE PREPARATION AND ANALYTICAL METHODS

All placer concentrate samples were processed by Overburden Drilling Management Limited, Ontario. A table concentrate was produced from the submitted sample and then micro-panned to recover fine-grained sediment; the table concentrate was processed through heavy liquid (SG 3.3), and ferromagnetic separations were prepared. PGM grains were hand picked and identified by SEM. Grains were mounted in a quick-setting araldite medium (~2.5-cm-diameter grain mount) and polished for analysis.

Electron-microprobe (EMP) analyses of the PGM were carried out using a JEOL JXA-8600 electron microprobe (A.D. Edgar Laboratory, University of Western Ontario, London, Ontario) in wavelength-dispersion spectrometry mode (WDS) at 25 kV and 30 nA, with a finely focused beam (<2 μm) and CITZAF on-line correction procedures. The following X-ray lines (and standards) were used: NiK α , FeK α , CoK α , CuK α , IrL α , PtL α , OsL α , RuL α , PdL β (pure metals), RhL α (synthetic Pt₉₀Rh₁₀), AsL α (FeAsS), and SK α (FeS). The PdL β line was used instead of PdL α in order to eliminate overlap between emission lines of Rh and Pd. We preferred to use the AsL α line, because the alternative K α line would overlap with lines of some of the heavy PGE. All possible peak-overlaps were examined and corrected during a careful analysis of relevant standards. The EMP data for silicates included in the PGM were obtained using WDS analysis at 15 kV and 20 nA, and a set of well-defined synthetic and natural mineral standards.

NOMENCLATURE OF Pt–Fe–(Cu–Ni)
AND IR–OS–RU ALLOYS

In accordance with existing nomenclature (Cabri & Feather 1975), three natural Pt–Fe alloys are presently recognized. Pt–Fe alloy with a disordered structure (*fcc*), space group *Fm3m*, is known as Fe-rich platinum [20–50 at.% Fe, and formerly “ferroan” platinum: Bayliss *et al.* (2005)] or “native Pt” (Fe < 20 at.% and Pt > 80 at.%). Isoferroplatinum, ideally Pt₃Fe, has an ordered primitive cubic (*pc*) structure, space group *Pm3m*, and typically contains 25 to 35 at.% Fe. Tetraferroplatinum (PtFe) is tetragonal, space group *P4/mmm*, and typically contains 45 to 55 at.% Fe and may also exhibit elevated levels of Cu (*e.g.*, 0.25 atoms

per formula unit, *apfu*; Cabri *et al.* 1977). A copper-bearing alloy, tulameenite (Pt₂FeCu), with an ordered tetragonal structure, was first described in PGE-bearing placers along the Tulameen River, which are associated with the Tulameen Alaskan-type complex (Cabri *et al.* 1973, Nixon *et al.* 1990). Tulameenite forms two solid-solution series: one with ferronickelplatinum (Pt₂FeNi; Rudashevsky *et al.* 1983), which is isostructural with tulameenite, and another with tetraferroplatinum (Nixon *et al.* 1990, Bowles 1990). In the system Os–Ir–Ru, the following species are recognized: *osmium*, hexagonal with Os as the major element, *iridium*, cubic with Ir dominant, *ruthenium*, hexagonal with Ru being the major element, and *rutheniridosmine*, hexagonal with Ir > Os or Ru (Harris & Cabri 1991).

RESULTS AND DISCUSSION

PGM species

A total of 70 PGM grains, varying from *ca.* 0.1 to 1.5 mm in cross section, were examined in the five samples of heavy-mineral concentrates (Fig. 1). Of the 70 grains analyzed, 47 represent various Pt–Fe–(Cu) alloys, and 23 are various alloys of Ir, Os, and Pt, some of which are enriched in Ru. Of the 47 Pt–Fe–(Cu) grains, 22 consist principally of Pt₃Fe-type alloys [with an atomic $\Sigma\text{PGE}:(\text{Fe} + \text{Cu} + \text{Ni})$ ratio of 2.5–3.5]: Fe-rich platinum or isoferroplatinum or both, 13 grains are Fe-rich Pt with $\Sigma\text{PGE}:(\text{Fe} + \text{Cu} + \text{Ni})$ of 3.6–5.6, five are members of the observed tetraferroplatinum–tulameenite series, and seven are “Pt₂Fe”-type alloy. Thus, the Pt₃Fe-type alloy dominates the Pt–Fe–(Cu) alloy population. Among the 23 grains of Ir–Os–(Pt–Ru) alloys, 14 are Ir-dominant alloy (*i.e.*, the mineral *iridium*), five are Os-dominant alloy (*osmium*), and four are Ru-enriched alloys, the composition of which is close to that of rutheniridosmine. In addition, Ir- and Os-dominant alloys occur as exsolution products in host Pt–Fe alloys.

Minor to trace amounts of PGE-bearing sulfides and sulfarsenides are intimately associated with the Pt–Fe alloys: cooperite (PtS), a PGE thiospinel enriched in Ni and corresponding to Ni-rich cuproiridsite [(Cu,Ni,Fe)(Ir,Rh,Pt)₂S₄], unusual sperrylite-type [(Pt,Rh,Fe)(As,S)_{2–x}] and platarsite-type [PtAs_{1–x}S_{1+x}, or unnamed Pt(S,As)_{2–x}] phases, and unnamed (Ir,Rh,Pt)S(?). In addition, minute inclusions of various anhydrous and hydrous silicates, including quartz, are present in some of the placer PGM grains. The compositions and characteristic textural features of these PGM are described below.

*Pt₃Fe-type alloys: Fe-rich platinum
or isoferroplatinum*

EMP analyses of Pt₃Fe-type alloys are given in Tables 1 and 2. The principal alloys have the composi-

tion (Pt,Ir,Rh)₃(Fe,Cu,Ni), which approximates the ideal isoferroplatinum (Pt₃Fe) composition (*e.g.*, Cabri & Feather 1975, Malitch & Thalhammer 2002), but in the absence of X-ray-diffraction data, we cannot distinguish Fe-rich platinum from isoferroplatinum. Placer grains of Pt₃Fe-type alloy(s) are subhedral, partly faceted to anhedral, up to 1.5 mm in size, and many grains display well-developed crystal faces (Figs. 2A, B). Some grains contain micro-inclusions or fine exsolution lamellae of various Os–Ir or Ir–Os–(Ru–Pt) alloys, which are locally abundant (Figs. 3A, 4A). Composite grains also are present and consist of Pt–Fe alloys (Pt₃Fe or “Pt₂Fe”) intergrown with Ir-dominant alloys, or zoned intergrowths of various Pt–Fe and Pt–Fe–Cu alloys. An example of an Ir-dominant alloy grain enclosing a droplet-like inclusion of Pt₃Fe is illustrated in Figure 3E. Such a texture is commonly interpreted to indicate entrapment in a liquid state.

In terms of *apfu*, calculated on the basis of $\Sigma \text{atoms} = 4$, the following compositional ranges in the Pt₃Fe-type alloys are observed, based on results of thirty-two WDS analyses (hereafter: $n = 32$): Pt 2.35–3.04, Ir 0–0.44, Rh 0.02–0.15, Os 0–0.07, Pd 0–0.13, Ru 0–0.02, Fe 0.57–1.10, Cu 0.005–0.35, and Ni 0–0.08, with ΣPGE and (Fe + Cu + Ni) values ranging from 2.84 to 3.12 and

from 0.88 to 1.16, respectively. The mean composition yields the formula [(Pt_{2.84}Ir_{0.05}Rh_{0.05}Pd_{0.03}Ru_{0.01})_{Σ2.99}(Fe_{0.88}Cu_{0.12}Ni_{0.01})_{Σ1.01}; $n = 32$], which is very close to being ideal, and displays equal proportions of Ir and Rh (0.05 *apfu* each), with an atomic Ir:Rh ratio of 1.0. From these EMP data, there appears to be a coupled substitution involving the replacement of (Ir + Rh + Pd) for Pt, and (Cu + Ni) for Fe (0.13 *apfu* each). However, the correlation (Ir + Rh + Pd) *versus* (Cu + Ni) is weak over the entire dataset [$n = 32$; correlation coefficient (R) = –0.39]. The correlation between Ir and Rh also is weak, although positive ($R = 0.42$). A positive Ir–Rh correlation (the R value was not given) was also noted by Tolstykh *et al.* (2002) in Pt–Fe alloys from the Salmon River placers, Goodnews Bay, Alaska, which are associated with the Red Mountain Alaskan-type complex.

The maximum contents of Ir and Rh in the analyzed Pt₃Fe-type alloys are 13.4 wt.% (10.9 at.%) and 2.5 wt.% (3.9 at.%), respectively ($n = 32$; Tables 1, 2) which deviate significantly from the mean composition. These abundances of Ir and Rh closely approach those reported in Pt₃Fe-type alloys from the Salmon River placers in Alaska (15.4 wt.% Ir and 2.3 wt.% Rh; Tolstykh *et al.* 2002). Most reported abundances of Ir

TABLE 1. COMPOSITIONS OF Pt–Fe–(Cu) ALLOYS (*apfu*) WITH $2.5 < \Sigma \text{PGE} : (\text{Fe} + \text{Cu} + \text{Ni}) < 3.5$ FROM PLACER DEPOSITS, BRITISH COLUMBIA

	Cu	Fe	Ni	Pt	Ir	Os	Pd	Rh	Ru	Total
12C 1	0.76	7.89	0.08	87.58	1.98	0.09	0.48	1.24	0.03	100.13
12C 2	0.71	9.33	0.28	82.64	5.01	0.14	1.19	1.02	0.00	100.32
12C 3	0.80	8.11	0.09	83.86	2.39	0.11	1.07	2.52	0.00	98.95
12C 4	0.75	8.28	0.29	87.63	0.84	0.09	0.03	0.51	0.02	98.44
16A 5	0.99	7.32	0.13	85.82	2.69	0.13	0.33	0.94	0.00	98.35
16A 6	0.61	7.27	0.02	87.72	0.00	0.19	0.81	0.75	0.00	97.37
16A 7	0.79	7.09	0.02	86.44	1.75	0.11	1.28	0.99	0.00	98.47
16A 8	0.57	7.41	0.01	88.33	0.00	0.14	1.17	1.00	0.00	98.63
16A 9	0.98	7.66	0.06	86.92	0.00	0.14	0.34	1.06	0.07	97.23
16A 10	1.32	6.30	0.03	87.82	0.00	0.37	0.69	1.42	0.03	97.98
16A 11	0.72	7.45	0.03	88.39	0.00	0.06	0.54	0.49	0.02	97.70
16A 12	2.37	5.31	0.07	87.19	0.00	1.53	0.03	0.32	0.28	97.10
16A 13	1.71	5.86	0.07	87.20	0.00	1.52	0.10	0.54	0.24	97.24
16A 14	0.78	7.28	0.00	87.43	0.47	0.25	0.07	0.79	0.00	97.07
16A 15	0.79	6.60	0.03	88.03	0.00	1.02	0.04	0.41	0.14	97.06
95A 16	0.43	9.07	0.12	79.42	8.26	0.47	0.32	1.38	0.02	99.49
95A 17	0.35	8.72	0.13	73.53	13.44	2.07	0.24	1.54	0.22	100.24
95A 18	0.05	9.83	0.04	87.36	2.54	0.02	0.00	0.29	0.04	100.17
40A 19	0.64	8.71	0.74	84.50	3.59	0.11	0.21	0.66	0.00	99.16
40A 20	0.55	8.90	0.60	85.73	1.96	0.01	0.05	0.49	0.00	98.30
40A 21	1.28	8.30	0.02	87.70	0.00	0.53	0.90	0.73	0.00	99.46
40A 22	1.97	7.06	0.04	88.24	0.00	0.16	2.21	0.49	0.04	100.21
40A 23	3.59	6.40	0.00	88.14	0.00	0.27	0.89	0.89	0.03	100.21
40A 24	0.89	8.14	0.02	88.94	0.00	0.11	0.54	0.54	0.00	99.18
16A 25	1.86	7.00	0.07	89.71	0.00	0.94	0.10	0.64	0.08	100.40
40A 26	1.56	7.77	0.02	88.36	0.00	0.11	0.90	0.73	0.00	99.45
40A 27	0.81	9.15	0.05	84.80	2.42	0.09	0.54	1.58	0.00	99.44
40A 28	2.13	7.88	0.00	87.53	0.00	0.08	0.73	0.85	0.06	99.26
40A 29	0.50	9.37	0.04	84.60	2.53	0.14	0.61	0.99	0.00	98.78
40A 30	0.51	9.92	0.07	84.07	2.51	0.01	0.64	0.89	0.02	98.64
40A 31	2.93	5.44	0.02	89.19	0.00	0.59	0.57	0.59	0.00	99.33
40A 32	3.13	4.91	0.00	89.67	0.00	0.47	0.65	0.58	0.08	99.49

Results of WDS analyses (JEOL–8600 electron microprobe); Co was not detected (<0.05 wt.%).

TABLE 2. ATOM PROPORTIONS IN Pt–Fe–(Cu) ALLOYS (*apfu*) WITH $2.5 < \Sigma \text{PGE} : (\text{Fe} + \text{Cu} + \text{Ni}) < 3.5$ FROM PLACER DEPOSITS, BRITISH COLUMBIA

	Pt	Ir	Os	Rh	Pd	Ru	Fe	Cu	Ni	$\Sigma \text{PGE} / (\text{Fe} + \text{Cu} + \text{Ni})$
1	71.14	1.63	0.07	1.91	0.72	0.05	22.39	1.89	0.20	3.08
2	64.70	3.98	0.11	1.52	1.71	0.00	25.52	1.72	0.74	2.57
3	67.51	1.95	0.09	3.85	1.58	0.00	22.81	1.98	0.24	3.00
4	71.92	0.70	0.08	0.80	0.05	0.03	23.74	1.88	0.80	2.79
5	71.44	2.28	0.11	1.48	0.51	0.00	21.28	2.54	0.36	3.13
6	74.24	0.00	0.16	1.20	1.26	0.00	21.49	1.58	0.06	3.32
7	72.16	1.49	0.10	1.56	1.96	0.00	20.67	2.02	0.05	3.40
8	73.50	0.00	0.12	1.58	1.78	0.00	21.54	1.46	0.02	3.34
9	72.57	0.00	0.12	1.68	0.52	0.11	22.34	2.50	0.16	3.00
10	74.19	0.00	0.32	2.27	1.07	0.05	18.59	3.43	0.07	3.53
11	74.46	0.00	0.05	0.78	0.84	0.03	21.92	1.86	0.07	3.19
12	75.16	0.00	1.35	0.52	0.05	0.47	15.99	6.26	0.21	3.45
13	74.93	0.00	1.34	0.88	0.16	0.39	17.59	4.52	0.19	3.48
14	74.34	0.40	0.22	1.27	0.11	0.00	21.62	2.03	0.00	3.23
15	76.01	0.00	0.90	0.68	0.07	0.24	19.91	2.10	0.10	3.52
16	63.58	6.71	0.39	2.10	0.46	0.03	25.36	1.05	0.32	2.74
17	58.81	10.91	1.70	2.33	0.35	0.33	24.36	0.87	0.33	2.91
18	69.77	2.06	0.02	0.44	0.00	0.06	27.42	0.12	0.11	2.62
19	67.75	2.92	0.09	1.00	0.30	0.00	24.39	1.57	1.97	2.58
20	69.41	1.61	0.01	0.75	0.07	0.00	25.17	1.36	1.62	2.55
21	70.56	0.00	0.44	1.12	1.32	0.01	23.33	3.17	0.06	2.77
22	70.97	0.00	0.13	0.75	3.26	0.07	19.84	4.87	0.11	3.03
23	70.42	0.00	0.22	1.35	1.30	0.04	17.86	8.81	0.00	2.75
24	72.72	0.00	0.09	0.84	0.81	0.00	23.25	2.24	0.05	2.92
25	73.18	0.00	0.78	0.99	0.14	0.13	19.95	4.66	0.18	3.03
26	71.55	0.00	0.09	1.12	1.34	0.00	21.98	3.88	0.04	2.86
27	67.33	1.95	0.07	2.38	0.79	0.01	25.38	1.96	0.13	2.64
28	70.17	0.00	0.07	1.29	1.08	0.09	22.07	5.24	0.00	2.66
29	67.85	2.06	0.11	1.51	0.90	0.00	26.25	1.22	0.10	2.63
30	66.74	2.02	0.01	1.33	0.93	0.03	27.51	1.24	0.18	2.46
31	74.30	0.00	0.51	0.93	0.87	0.00	15.83	7.50	0.06	3.28
32	75.12	0.00	0.40	0.92	1.00	0.12	14.37	8.05	0.01	3.46

The analytical results (in wt.%) are listed in Table 1.

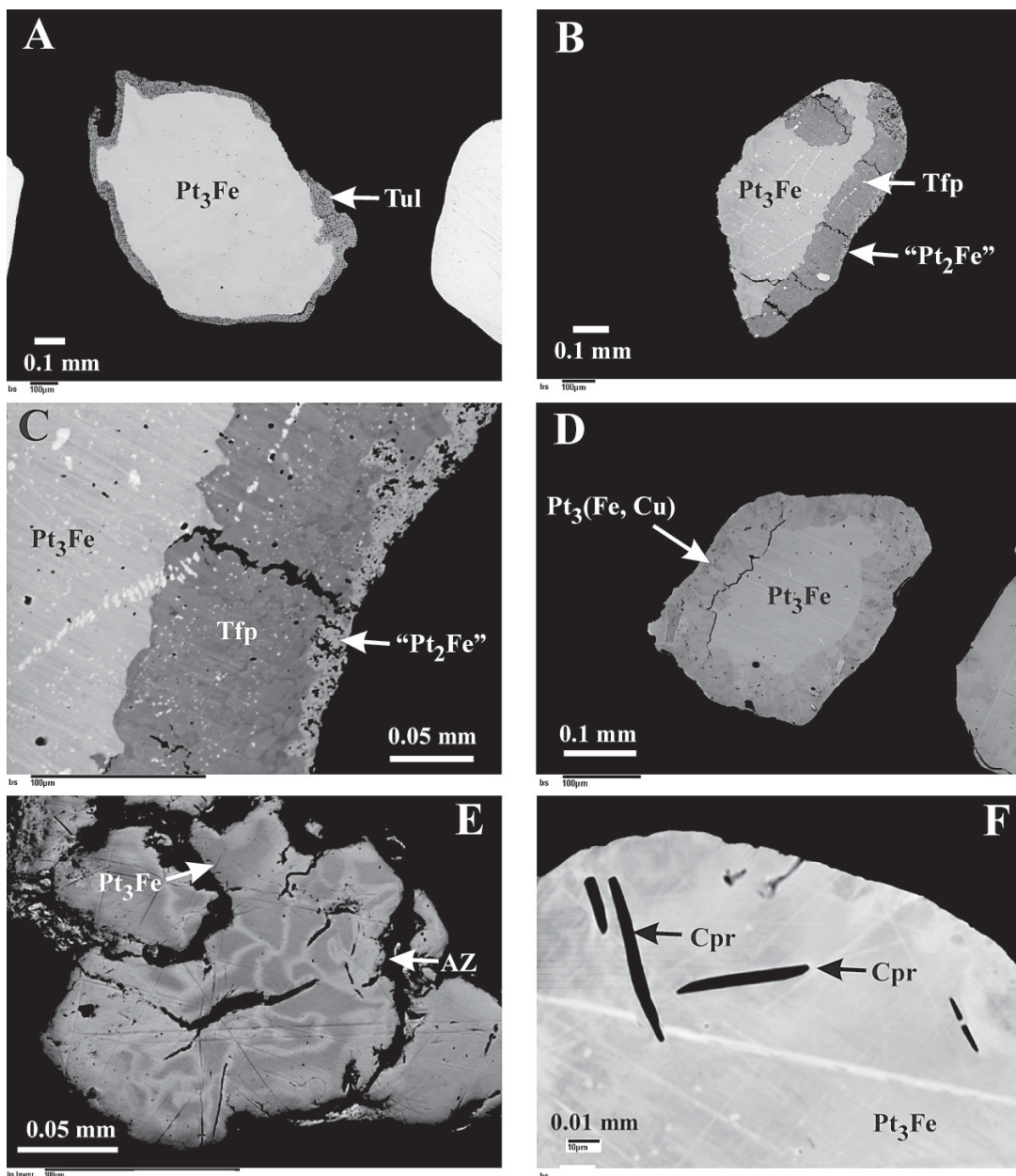


FIG. 2. A. A subhedral grain of Pt_3Fe -type alloy mantled by a narrow and porous rim of members of the tulameenite–ferro-nickelplatinum series [Tul: $(Pt_{1.97-1.98}Ir_{0.02}Rh_{0.02})_{\Sigma 2.00-2.02}Fe_{0.92-0.99}(Cu_{0.63-0.73}Ni_{0.35-0.37})_{\Sigma 1.00-1.08}$]. B. A subhedral grain of Pt_3Fe -type alloy, which is partly mantled by a Cu-rich variety of tetraferroplatinum, Tfp [$(Pt_{0.98}Ir_{0.04}Rh_{0.02})_{\Sigma 1.04}(Fe_{0.74}Cu_{0.20}Ni_{0.01})_{\Sigma 0.95}$; gray rim]. Note the presence of a very narrow “ Pt_2Fe ” rim [$(Pt_{1.92}Ir_{0.08}Rh_{0.02})_{\Sigma 2.02}(Fe_{0.91}Cu_{0.06}Ni_{0.01})_{\Sigma 0.98}$], which is developed after the tetraferroplatinum rim. C. Magnification of Figure 2B, showing the outer “ Pt_2Fe ” rim, which is somewhat porous, and has an irregular boundary with the tetraferroplatinum rim (Tfp). D. A subhedral grain of Pt_3Fe -type alloy poor in Cu [$(Pt_{3.04}Os_{0.04}Rh_{0.03}Ru_{0.01})_{\Sigma 3.12}(Fe_{0.80}Cu_{0.08})_{\Sigma 0.88}$], which compositionally ranges up to Fe-rich platinum with the atomic PGE:(Fe + Cu + Ni) ratio of 4.3. These Cu-poor Pt–Fe alloys are mantled by a $Pt_3(Fe,Cu)$ alloy enriched in Cu [e.g., $(Pt_{2.93}Rh_{0.04}Os_{0.03})_{\Sigma 3.00}(Fe_{0.80}Cu_{0.19})_{\Sigma 0.99}$; gray]. E. An anhedral grain of Pt_3Fe -type alloy (original alloy: dark gray), consisting of alteration zones (AZ), which are rim- and veinlet-like zones (light gray). F. Exsolution lamellae of Ni-rich cuproiridsite (Cpr: black), which are “crystallographically” oriented almost perpendicular to each other in the host Pt_3Fe -type alloy. Figures 2A–F are back-scattered-electron images.

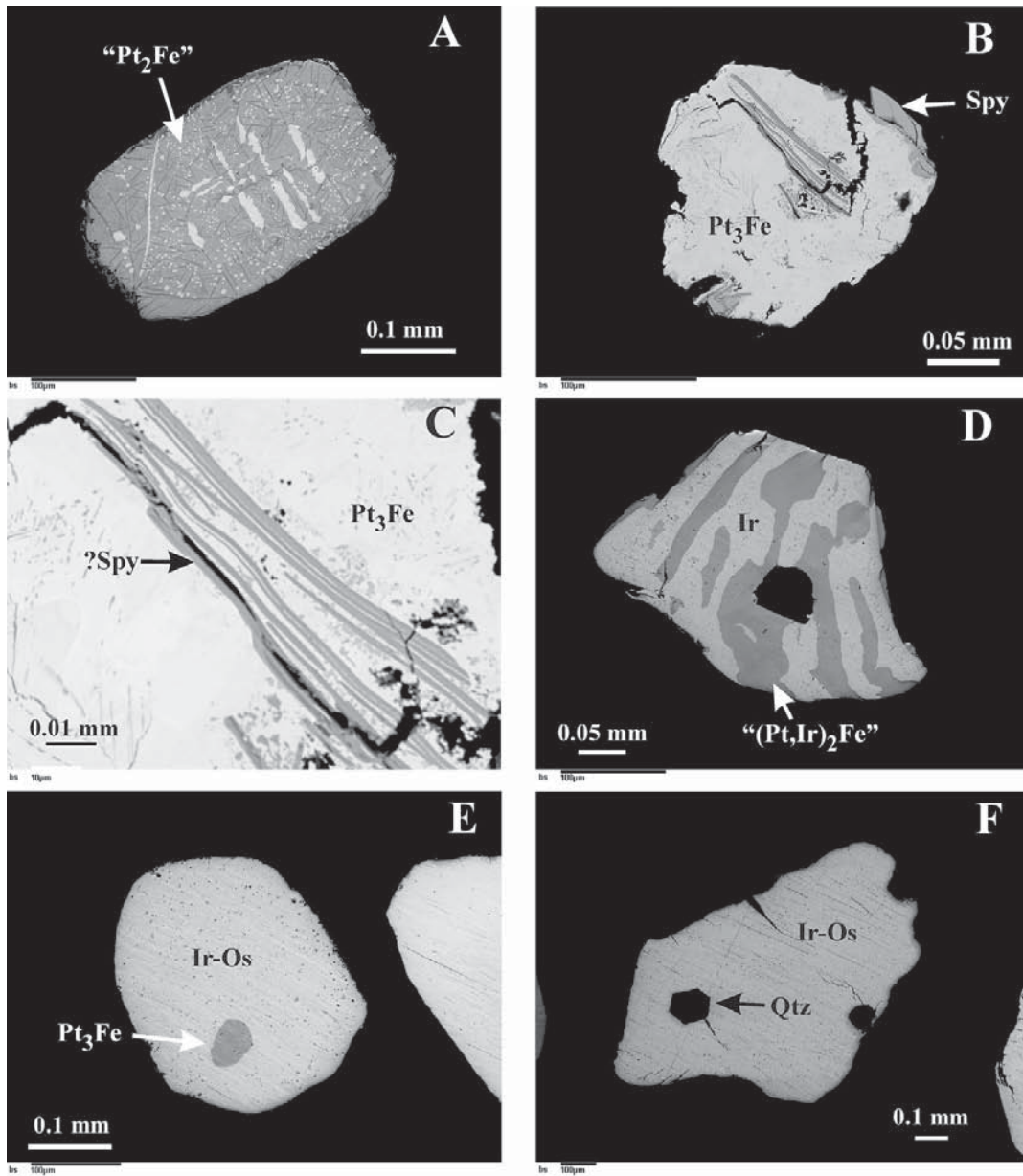


FIG. 3. A. "Crystallographically" oriented lamellae of Ir-dominant alloy [white: $\text{Ir}_{71.02-71.10}\text{Os}_{9.51-9.61}\text{Pt}_{7.34-7.37}\text{Fe}_{5.08-5.18}\text{Rh}_{3.29-3.44}\text{Ru}_{3.14-3.26}\text{Ni}_{0.25-0.28}$], enclosed by heterogeneous "Pt₂Fe" alloy [(Pt_{1.65}Ir_{0.21}Rh_{0.04}Pd_{0.01})_{Σ1.91}(Fe_{1.00}Cu_{0.05}Ni_{0.04})_{Σ1.09}: gray]. B. A blocky grain of Rh-Fe-S-bearing sperrylite (Spy), which occurs at the margin of Pt₃Fe-type alloy. Note that lamellar grains or veinlets of this sperrylite-type phase (?) are also present close to the center of the host Pt-Fe alloy grain. C. Subparallel orientation of the sperrylite-type phase (?) enclosed within the Pt₃Fe-type alloy (Fig. 3B). D. A subhedral composite grain of Ir-Pt-Os alloy [Ir, white: $\text{Ir}_{72.52}\text{Pt}_{8.30}\text{Os}_{7.13}\text{Fe}_{5.92}\text{Ru}_{3.70}\text{Rh}_{2.18}\text{Ni}_{0.25}$], that displays evidence of exsolution of "(Pt,Ir)₂Fe" [(Pt_{1.72}Ir_{0.21}Rh_{0.03})_{Σ1.96}(Fe_{0.98}Cu_{0.04}Ni_{0.01})_{Σ1.03}: gray] within this Ir-Pt-Os alloy. Note that these "(Pt,Ir)₂Fe" lamellae are oriented roughly subparallel to each other and also to crystal faces of the host Ir-rich alloy. A two-mineral silicate inclusion (diopside and ferro-edenite: anal. 1,3, Table 12) is present in the center of this grain. E. A grain of Ir-Os-Pt alloy [Ir_{51.37}Os_{33.53}Pt_{7.02}Ru_{4.07}Rh_{3.16}Fe_{0.80}Ni_{0.05}] containing a droplet-like inclusion of a Pt₃Fe-type alloy (gray). The upper portion of this grain is subrounded in cross-section, whereas its lower part displays preserved crystal faces. F. A large grain of Ir-Os-Pt alloy [Ir_{59.10}Os_{18.82}Pt_{14.12}Ru_{3.82}Rh_{2.03}Fe_{1.92}Ni_{0.15}] contains a euhedral inclusion of quartz (Qtz). Figures 3A-F are back-scattered-electron images.

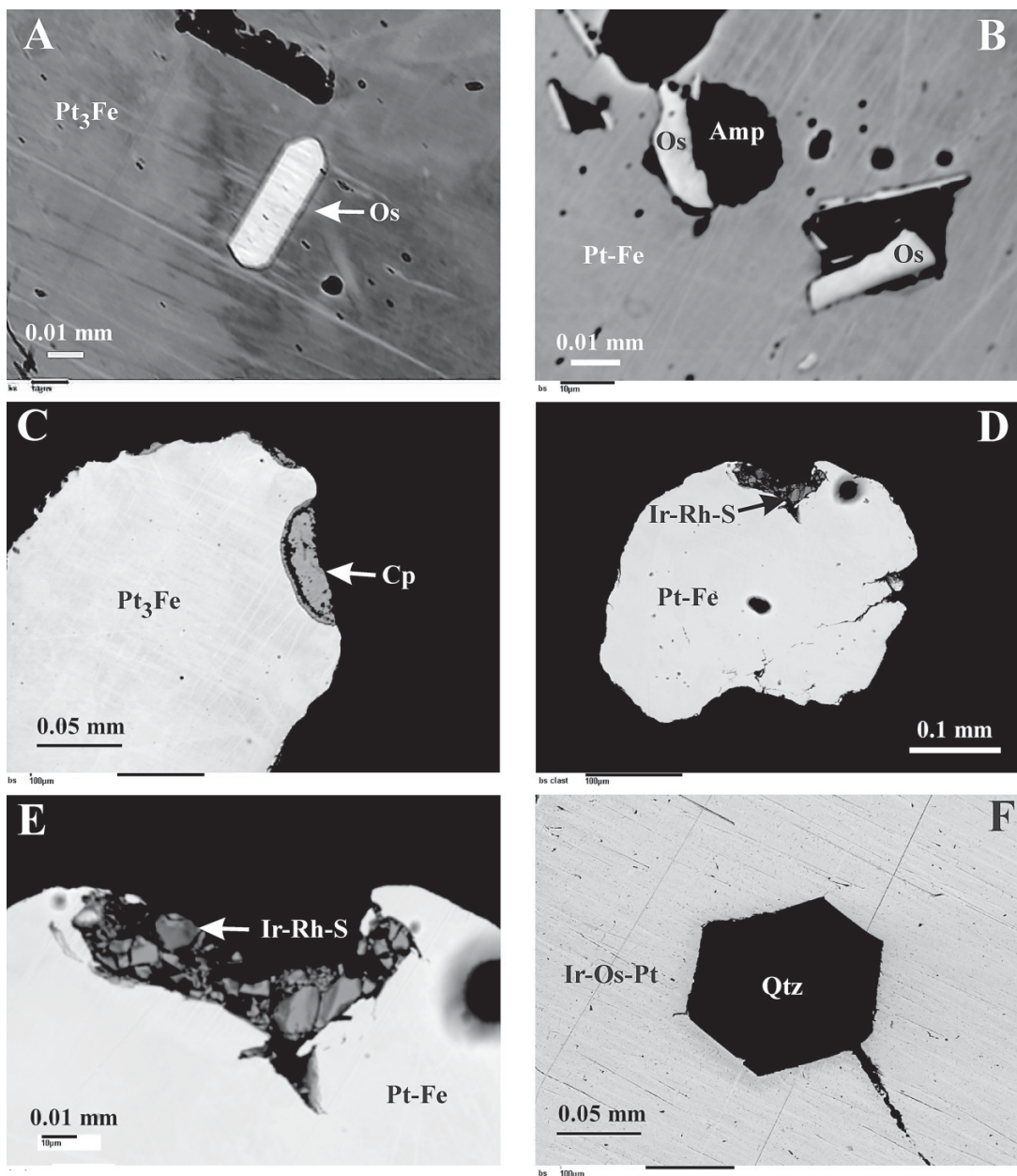


FIG. 4. A. A well-formed hexagonal crystal of native Os [$\text{Os}_{98.67}\text{Pt}_{0.81}\text{Rh}_{0.25}\text{Pd}_{0.25}\text{Fe}_{0.02}$] enclosed by an anhedral grain of Pt_3Fe -type alloy [$(\text{Pt}_{2.91}\text{Rh}_{0.03}\text{Pd}_{0.03})_{\Sigma 2.97}(\text{Fe}_{0.93}\text{Cu}_{0.09})_{\Sigma 1.02}$]. B. Minute crystals of native Os [$\text{Os}_{87.64}\text{Ir}_{6.60}\text{Ru}_{2.49}\text{Pt}_{1.66}\text{Rh}_{1.14}\text{Fe}_{0.19}\text{Pd}_{0.13}$; labeled "Os"] in intergrowth with a potassian sodic-calcic amphibole (Amp; anal. 4, Table 12), which are enclosed within Fe-rich Pt with the atomic PGE:(Fe + Cu + Ni) ratio of 4.0 (Pt-Fe). C. A narrow rim of cooperite (Cp), which is developed around a Pt_3Fe -type alloy grain. D. Fragments of a broken grain of Ir-Rh sulfide [unnamed (Ir,Rh)S(?)], which are preserved at the margin of a Pt-Fe alloy grain. Details of these fragments are shown in Figure 4E, which is a further magnification of Figure 4D. F. Magnification of the quartz inclusion (Qtz), which is observed in the Ir-Os-(Pt) alloy shown in Figure 3F. Figures 4A-F are back-scattered-electron images.

in Pt–Fe alloys are lower, with the exception of Pt–Fe alloy from the Saskatchewan River placer, Alberta (22.97 wt.% Ir; Cabri *et al.* 1996), for example, or an Ir-dominant analogue of isoferroplatinum (chengdeite) from the Luanhe River placer, China (Yu 1995). Iridium clearly substitutes for Pt and forms a well-defined negative Ir *versus* Pt correlation ($R = -0.88$; Fig. 5).

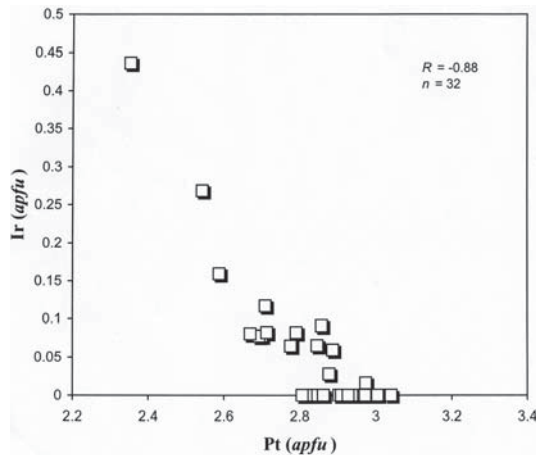


FIG. 5. A Pt–Ir correlation (in atoms per formula unit, *apfu*; $\Sigma_{\text{atoms}} = 4$) in electron-microprobe-derived compositions of Pt₃Fe-type alloys from placer deposits, British Columbia (this study).

The content of PGE and of base metals, and the atomic $\Sigma\text{PGE}:(\text{Fe} + \text{Cu} + \text{Ni})$ ratio, show variations (Tables 1, 2, Fig. 6); the atomic proportions of minor Ir, Rh and Pd are generally close to those observed in related alloys from Alaska (Fig. 7; *cf.* Tolstykh *et al.* 2002). The mean content of Cu in analyzed Pt₃Fe-type alloys is 1.2 wt.% (Tables 1, 2), which is identical to the mean content of Cu in similar alloys [Pt_{2.5}(Fe,Ni,Cu)_{1.5}] associated with the Tulameen Alaskan-type complex (Nixon *et al.* 1990). The maximum Cu content (3.6 wt.%; $n = 32$) is somewhat greater than that reported in Pt₃Fe-type alloys from Alaska (up to 1.15 wt.% Cu; Tolstykh *et al.* 2002). Copper contents are negatively correlated with Fe ($R = -0.83$; $n = 32$), indicative of Cu-for-Fe substitution. Ni contents are generally low and have a maximum value of 0.74 wt.% (Table 1), somewhat greater than the amount of Ni observed in a Pt₃Fe-type alloy from Alaska (0.33 wt.% Ni; Tolstykh *et al.* 2002). The Pt–Fe alloys associated with the Tulameen complex are richer in Ni (1.2 to 3.2 wt.%; Nixon *et al.* 1990), as are Pt₃Fe-type alloys (4.8 to 7.2 wt.% Ni) from the Kytlym Alaskan-type complex, Urals. However, the Cu content of these Uralian alloys (1.3 to 2.35 wt.%, Garuti *et al.* 2002) is similar to those of the Pt–Fe alloys analyzed in this study (Tables 1, 2). Compositions of Pt-rich alloys with higher values of the ratio $\Sigma\text{PGE}:(\text{Fe} + \text{Cu} + \text{Ni})$, ranging from 3.6 to 5.6, correspond to Fe-rich Pt (Tables 3, 4). One of these alloy samples contains 80.5 at.% Pt (anal. 9, Table 4); it is “native platinum”, a variety of Fe-rich platinum (Cabri & Feather 1975).

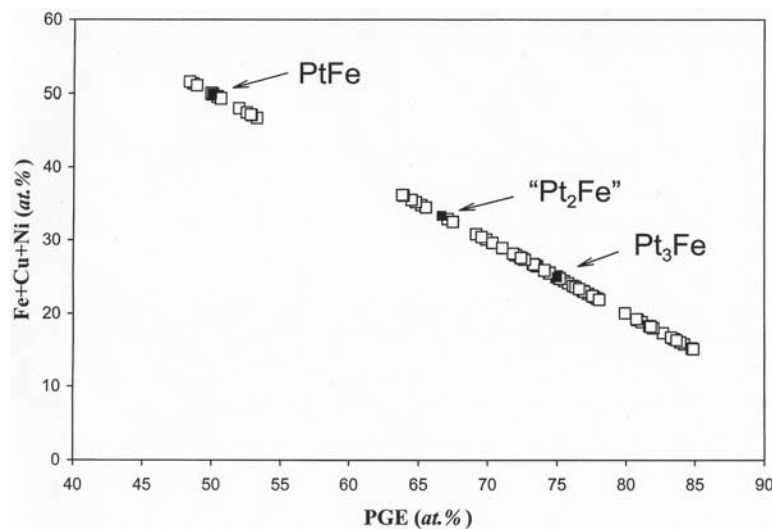


FIG. 6. Compositional variations (in at.%) of the analyzed Pt–Fe–(Cu) alloys from placer deposits, British Columbia, in terms of the plot of ΣPGE *versus* (Fe + Cu + Ni). Compositions of ideal Pt₃Fe, “Pt₂Fe” and PtFe are shown for comparison (filled symbols).

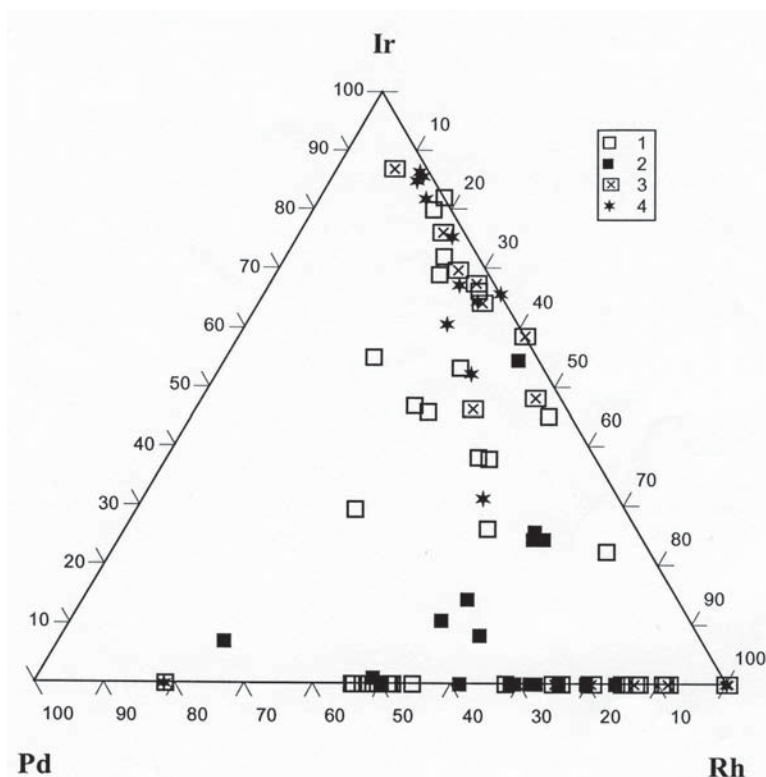


Fig. 7. Contents of minor elements (Pd, Ir, and Rh) in various Pt-Fe-(Cu) alloys from placer deposits, British Columbia. The following symbols are used in this diagram: (1) Pt₃Fe-type alloys, (2) Fe-rich Pt with the Σ PGE:(Fe + Cu + Ni) ratio of 3.6–5.6, (3) members of the tetraferroplatinum–tulameenite series, and (4) “Pt₂Fe”-type alloys. Note that these data points generally extend along the Ir–Rh and Rh–Pd joins, and, in contrast, the Pd–Ir join is clearly avoided.

“Pt₂Fe”-type alloys

Some of the analyzed grains of Pt–Fe alloy have an atomic Σ PGE:(Fe + Cu + Ni) ratio close to 2 (Tables 5, 6). In the Σ PGE–(Fe + Cu + Ni) diagram (Fig. 6), these compositions fall on a line between ideal Pt₃Fe and PtFe. Although the existence of “Pt₂Fe” is not reported in the Pt–Fe system because of a miscibility gap (Cabri & Feather 1975), natural “Pt₂Fe”-type alloys have been reported from several localities (Johan *et al.* 1989, Malitch & Thalhammer 2002, Oberthür *et al.* 2002). In addition, Nixon *et al.* (1990) have reported a Pt_{2.5}(Fe,Ni,Cu)_{1.5} alloy derived from the Tulameen complex. In some cases, the naturally occurring “Pt₂Fe” may represent a submicroscopic intergrowth of Pt₃Fe and PtFe (<1 μ m in size) exsolved upon cooling within the miscibility gap (*e.g.*, Zhernovskiy *et al.* 1985), including some of the observed “Pt₂Fe” composition of the placer grains (*e.g.*, Fig. 3A) and of the narrow rim (Fig. 2C). One composite alloy grain, however,

appears to consist of a single “(Pt,Ir)₂Fe” phase. It forms a generally subparallel “crystallographically” oriented intergrowth (Fig. 3D). Malitch & Thalhammer (2002) recently described examples of “homogeneous Pt₂Fe”, having a disordered *fcc* structure.

We suggest that the “(Pt,Ir)₂Fe” alloy (Fig. 3D), which is enriched in Ir [(Pt_{1.72}Ir_{0.21}Rh_{0.03}) Σ 1.96(Fe_{0.98}Cu_{0.04}Ni_{0.01}) Σ 1.03] and coexists with an Ir-dominant alloy enriched in Pt [Ir_{72.5}Pt_{8.3}Os_{7.1}Fe_{5.9}Ru_{3.7}Rh_{2.2}], could have formed by exsolution from a complex primary solid-solution at a high temperature. This mode of origin may have been a significant factor in stabilizing the “(Pt,Ir)₂Fe” alloy phase and the incorporation of substantial Ir.

Tulameenite–tetraferroplatinum series: deviations from ideal stoichiometry

The results of EMP analyses of alloys belonging to the tulameenite–tetraferroplatinum solid-solution series

are given in Tables 7 and 8. Most of the placer grains examined in this series (*ca.*, 0.1 to 0.5 mm across) are texturally heterogeneous, with abundant fractures. Relics of “Pt₂Fe” are locally preserved in some of these grains. Nickel is a not uncommon component of tulameenite from various localities. The maximum Ni content observed in this study (4.3 wt.%: Table 7) is close to that reported in tulameenite from the Tulameen

River placer (3.8 wt.% Ni, Cabri *et al.* 1996), and to that in tulameenite hosted *in situ* by chromitite of the Tulameen complex (2.9 wt.% Ni, Nixon *et al.* 1990). Tolstykh *et al.* (2002) reported up to 2.6 wt.% Ni in members of the tulameenite–tetraferroplatinum series from Alaska. A Ni–(Cu)-rich Pt–Fe alloy, believed to be tetraferroplatinum [Pt_{0.97}Pd_{0.03}]_{Σ1.00}(Fe_{0.66}Cu_{0.25}Ni_{0.10})_{Σ1.01}, was also reported from the Wellgreen intrusion, Yukon (Barkov *et al.* 2002).

Our EMP data (Tables 7, 8, Figs. 8A–F) lead to some original observations. The ideal scheme of element substitutions requires an atomic Pt:(Fe + Cu + Ni) ratio of 1.0 in members of the tulameenite–tetraferroplatinum [Pt₂FeCu–“Pt₂FeFe”] series. However, the ΣPGE:(Fe + Cu + Ni) ratio observed in the analyzed placer grains is 0.94–1.14, which deviates from the ideal (Tables 7, 8, Fig. 8B), and is positively correlated with Fe

TABLE 3. COMPOSITIONS OF Pt–Fe–(Cu) ALLOYS (*apfu*) WITH 3.6 < ΣPGE : (Fe+Cu+Ni) < 5.6 FROM PLACER DEPOSITS, BRITISH COLUMBIA

		Cu	Fe	Ni	Pt	Ir	Os	Pd	Rh	Ru	Total
12C	1	0.57	4.60	0.03	90.49	0.00	1.11	0.62	1.33	0.11	98.86
16A	2	0.98	5.06	0.04	88.60	0.00	0.99	0.60	1.31	0.18	97.76
16A	3	0.74	5.38	0.02	88.53	0.00	0.23	1.17	1.79	0.05	97.91
16A	4	0.41	4.47	0.09	89.83	0.00	0.89	0.39	1.97	0.12	98.17
16A	5	0.68	5.62	0.03	88.72	0.21	0.29	1.15	0.38	0.04	97.12
16A	6	1.29	4.17	0.03	88.64	0.40	1.13	0.74	1.07	0.22	97.69
16A	7	0.81	4.83	0.05	89.70	0.00	0.81	0.41	0.86	0.12	97.59
16A	8	0.99	5.21	0.02	88.49	0.13	0.90	0.29	0.52	0.31	96.86
16A	9	0.48	4.30	0.08	89.14	0.00	1.48	0.35	1.31	0.11	97.25
16A	10	0.39	5.17	0.07	86.37	4.75	1.12	0.15	1.97	0.32	100.31
40A	11	1.25	4.97	0.04	91.93	0.00	0.33	0.47	1.01	0.06	100.06
16A	12	1.94	5.12	0.05	88.91	0.06	0.64	1.57	1.44	0.20	99.93
40A	13	3.47	4.37	0.03	89.71	0.00	0.39	0.67	0.65	0.00	99.29
#93	14	0.42	5.52	0.05	91.97	0.00	0.17	0.28	0.83	0.02	99.26
#93	15	0.46	5.58	0.07	91.68	0.00	0.16	0.35	0.89	0.00	99.19
#93	16	0.43	5.55	0.09	91.96	0.00	0.14	0.34	0.83	0.03	99.37
#93	17	0.36	4.83	0.04	89.42	1.15	0.30	0.37	1.53	0.06	98.06
#93	18	0.35	4.96	0.04	89.50	1.17	0.33	0.42	1.52	0.12	98.41
#93	19	0.39	4.92	0.07	89.85	1.28	0.32	0.41	1.57	0.10	98.91
#93	20	0.90	5.54	0.09	87.17	0.77	0.81	0.90	1.58	0.37	98.13

Results of WDS analyses (JEOL–8600 electron microprobe); Co was not detected (<0.05 wt.%).

TABLE 4. ATOM PROPORTIONS IN Pt–Fe–(Cu) ALLOYS (*apfu*) WITH 3.6 < ΣPGE : (Fe+Cu+Ni) < 5.6 FROM PLACER DEPOSITS, BRITISH COLUMBIA

		Pt	Ir	Os	Rh	Pd	Ru	Fe	Cu	Ni	ΣPGE / (Fe+Cu+Ni)
1		79.80	0.00	1.01	2.22	1.00	0.19	14.17	1.54	0.08	5.33
2		77.47	0.00	0.89	2.17	0.96	0.31	15.46	2.62	0.13	4.49
3		76.62	0.00	0.20	2.94	1.86	0.09	16.26	1.98	0.05	4.47
4		79.81	0.00	0.81	3.31	0.63	0.20	13.87	1.11	0.26	5.56
5		77.85	0.19	0.26	0.63	1.85	0.07	17.23	1.83	0.09	4.22
6		78.70	0.36	1.03	1.80	1.21	0.37	12.93	3.52	0.08	5.05
7		79.61	0.00	0.74	1.45	0.66	0.21	14.97	2.21	0.15	4.77
8		78.35	0.12	0.82	0.87	0.46	0.53	16.11	2.68	0.06	4.30
9		80.50	0.00	1.37	2.25	0.57	0.18	13.56	1.33	0.23	5.61
10		74.18	4.14	0.98	3.20	0.23	0.53	15.51	1.04	0.19	4.97
11		78.93	0.00	0.29	1.64	0.73	0.09	14.91	3.29	0.11	4.46
12		74.34	0.05	0.55	2.28	2.40	0.32	14.95	4.97	0.14	3.98
13		75.65	0.00	0.34	1.04	1.04	0.00	12.87	8.98	0.08	3.56
14		79.98	0.00	0.15	1.37	0.44	0.03	16.77	1.12	0.14	4.55
15		79.51	0.00	0.15	1.46	0.56	0.00	16.90	1.22	0.19	4.46
16		79.71	0.00	0.13	1.36	0.54	0.05	16.80	1.15	0.26	4.49
17		79.34	1.04	0.27	2.58	0.60	0.11	14.97	0.98	0.12	5.22
18		78.90	1.04	0.30	2.54	0.68	0.20	15.27	0.94	0.13	5.12
19		78.81	1.14	0.28	2.60	0.66	0.17	15.07	1.04	0.22	5.12
20		74.79	0.67	0.71	2.56	1.41	0.61	16.60	2.37	0.26	4.20

The analytical results (in wt.%) are listed in Table 3.

TABLE 5. COMPOSITIONS OF Pt–Fe–(Cu) ALLOYS (*apfu*) WITH 1.8 < ΣPGE : (Fe+Cu+Ni) < 2.4 FROM PLACER DEPOSITS, BRITISH COLUMBIA

		Cu	Fe	Ni	Pt	Ir	Os	Pd	Rh	Ru	Total
95A	1	1.38	12.08	0.16	82.27	3.69	0.07	0.16	0.80	0.03	100.64
95A	2	0.43	10.87	0.15	85.56	1.14	0.02	0.39	0.95	0.01	99.52
40A	3	0.63	12.53	0.18	76.97	9.19	0.04	0.07	0.74	0.05	100.40
40A	4	0.63	12.85	0.19	76.13	9.43	0.03	0.09	0.70	0.05	100.10
40A	5	0.64	12.99	0.17	76.09	9.07	0.04	0.15	0.70	0.02	99.87
40A	6	4.73	9.15	0.51	83.34	1.13	0.16	0.00	0.31	0.01	99.34
40A	7	1.80	10.14	0.58	85.14	1.33	0.26	0.05	0.34	0.00	99.64
40A	8	1.09	9.34	0.79	83.10	0.00	0.11	3.75	0.82	0.00	99.00
40A	9	1.73	8.99	0.49	82.22	3.98	0.11	0.37	1.02	0.06	98.97
95A	10	0.82	11.27	0.15	83.40	3.23	0.12	0.05	0.51	0.05	99.60
40A	11	0.71	12.90	0.54	74.56	9.49	0.05	0.18	0.95	0.04	99.42
40A	12	0.36	10.35	0.18	83.89	3.00	0.12	0.35	1.12	0.03	99.40
40A	13	0.56	10.50	0.13	87.32	0.00	0.65	0.00	0.41	0.00	99.57

Results of WDS analyses (JEOL–8600 electron microprobe); Co was not detected (<0.05 wt.%).

TABLE 6. ATOM PROPORTIONS IN Pt–Fe–(Cu) ALLOYS (*apfu*) WITH 1.8 < ΣPGE : (Fe+Cu+Ni) < 2.4 FROM PLACER DEPOSITS, BRITISH COLUMBIA

		Pt	Ir	Os	Rh	Pd	Ru	Fe	Cu	Ni	ΣPGE / (Fe+Cu+Ni)
1		60.98	2.78	0.06	1.13	0.22	0.04	31.28	3.14	0.39	1.87
2		66.29	0.90	0.01	1.40	0.56	0.02	29.42	1.03	0.37	2.24
3		57.32	6.95	0.03	1.04	0.10	0.08	32.60	1.45	0.44	1.90
4		56.48	7.10	0.02	0.98	0.13	0.07	33.30	1.44	0.47	1.84
5		56.40	6.82	0.03	0.99	0.21	0.03	33.64	1.46	0.42	1.82
6		62.46	0.86	0.12	0.44	0.00	0.01	23.96	10.88	1.26	1.77
7		65.31	1.03	0.20	0.50	0.06	0.00	27.17	4.24	1.49	2.04
8		63.80	0.00	0.09	1.19	5.28	0.00	25.05	2.58	2.02	2.37
9		64.51	3.17	0.09	1.52	0.54	0.09	24.64	4.17	1.28	2.32
10		63.99	2.52	0.10	0.74	0.07	0.07	30.21	1.92	0.39	2.08
11		55.03	7.11	0.04	1.33	0.24	0.06	33.26	1.61	1.33	1.76
12		65.68	2.38	0.09	1.66	0.50	0.05	28.31	0.86	0.47	2.37
13		68.44	0.00	0.52	0.61	0.00	0.00	28.75	1.35	0.34	2.29

The analytical results (in wt.%) are listed in Table 5.

(Fig. 8C) and negatively with (Cu + Ni) (Fig. 8D). Also, the Σ PGE value of this series in the analyzed grains exhibits a notable departure (up to 2.13) from the ideal value of 2.0, and is positively correlated with Fe (Fig. 8E) and negatively with (Cu + Ni) (Fig. 8F). Although these deviations are quite minor, they are unlikely to reflect analytical error, since compositions of this series from Alaska (Tolstikh *et al.* 2002) lie along the same trend (Figs. 8A–F). It is noteworthy that the PGE-rich members of the tulameenite–tetraferroplatinum series from British Columbia [PGE $_{\Sigma 2.13}$ (Fe $_{1.54}$ Cu $_{0.32}$ Ni $_{0.01}$) $_{\Sigma 1.87}$: this study] and Alaska [PGE $_{\Sigma 2.09}$ (Fe $_{1.36}$ Cu $_{0.32}$ Ni $_{0.23}$) $_{\Sigma 1.91}$: recalculated from Tolstikh *et al.* 2002] display about the same degree of deviation from the ideal stoichiometry. These compositional data thus imply that members of the tulameenite–tetraferroplatinum series are somewhat nonstoichiometric and extend toward PGE $_{1+x}$ (Fe,Cu,Ni) $_{1-x}$, where $0 < x < 0.1$, rather than toward ideal PGE(Fe,Cu,Ni) compositions.

The presence of “Pt₂Fe” relics in the tulameenite–tetraferroplatinum grains implies a secondary origin, consistent with a late-stage deuteric event, such as serpentinization, for example (*cf.*, Cabri & Genkin 1991). Thus, the pre-existing Pt–Fe alloy(s) may have reacted with a late fluid rich in Cu to form members of the tulameenite–tetraferroplatinum series.

Zoned intergrowths of Pt–Fe–Cu alloys

Some placer grains of Pt–Fe–Cu alloys are zoned. For example, a subhedral grain of Pt₃Fe-type alloy (Fig. 2A) has a relatively Cu-poor core [(Pt $_{2.88}$ Ir $_{0.03}$ Rh $_{0.03}$) $_{\Sigma 2.94}$ (Fe $_{0.95}$ Cu $_{0.08}$ Ni $_{0.03}$) $_{\Sigma 1.06}$: anal. 4, Tables 1, 2] and is mantled by a narrow rim of tulameenite enriched in Ni: *ca.* 37% of the ferronickelplatinum component [(Pt $_{1.97-1.98}$ Ir $_{0.02}$ Rh $_{0.02}$) $_{\Sigma 2.00-2.02}$ Fe $_{0.92-0.99}$ (Cu $_{0.63-0.73}$ Ni $_{0.35-0.37}$) $_{\Sigma 1.00-1.08}$: anal. 1, 2, Tables 7, 8]. The porous texture of this rim (Fig. 2A) is consistent with

TABLE 7. COMPOSITIONS OF Pt–Fe–(Cu) ALLOYS (*apfu*) WITH $0.9 < \Sigma$ PGE : (Fe+Cu+Ni) < 1.1 FROM PLACER DEPOSITS, BRITISH COLUMBIA

		Cu	Fe	Ni	Pt	Ir	Os	Pd	Rh	Ru	Total
12C	1	7.79	10.79	4.28	75.22	0.79	0.19	0.03	0.42	0.00	99.51
12C	2	9.12	10.14	4.10	76.32	0.00	0.00	0.13	0.36	0.00	100.17
95A	3	3.96	16.73	0.16	73.30	5.17	0.00	0.11	1.22	0.00	100.65
95A	4	3.95	16.96	0.19	72.45	5.56	0.10	0.18	1.10	0.09	100.58
95A	5	10.71	12.26	0.57	76.77	0.00	0.09	0.03	0.28	0.00	100.71
40A	6	7.28	14.43	0.19	70.56	6.44	0.19	0.15	0.92	0.02	100.18
40A	7	13.09	9.91	0.58	74.49	1.01	0.32	0.00	0.38	0.00	99.78
40A	8	14.72	9.54	0.39	74.56	0.00	0.41	0.00	0.32	0.00	99.94
40A	9	12.46	11.13	0.60	73.47	0.00	0.23	0.06	0.22	0.00	98.17
40A	10	10.74	10.71	1.36	71.18	4.77	0.11	0.15	0.24	0.00	99.26
12C	11	9.00	11.30	4.14	76.73	0.00	0.00	0.05	0.30	0.00	101.52
95A	12	4.96	16.30	0.19	75.29	2.85	0.54	0.08	0.76	0.08	101.05
40A	13	1.91	18.04	0.61	75.34	1.79	0.09	0.29	0.82	0.00	98.89

Compositions 1 to 13: members of the tulameenite–tetraferroplatinum solid-solution series. Co was not detected (<0.05 wt.%).

the presence of abundant microvolumes of a fluid phase that possibly became concentrated in the environment at the final stage of crystallization.

The composite grain shown in Figure 2B has a core of Cu-poor isoferroplatinum or Fe-rich platinum (in at. %) [Pt $_{58.8-63.6}$ Ir $_{6.7-10.9}$ Rh $_{2.1-2.3}$ Os $_{0.4-1.7}$ Pd $_{0.4-0.5}$ Fe $_{24.4-25.4}$ Cu $_{0.9-1.1}$ Ni $_{0.3}$] (anal. 16, 17, Tables 1, 2). Replacement zones in this grain (*i.e.*, the “gray rim”: Fig. 2B) consist of a tetraferroplatinum-type alloy enriched in Cu [Pt $_{47.4-49.1}$ Ir $_{1.9-3.7}$ Rh $_{1.0-1.5}$ Os $_{0.0-0.4}$ Pd $_{0.1-0.2}$ Fe $_{37.2-38.8}$ Cu $_{7.9-9.9}$ Ni $_{0.4}$] (anal. 3, 4, 12, Tables 7, 8). In addition, this “gray rim” of tetraferroplatinum is partly mantled by an irregular and narrow “outer rim” (Figs. 2B, C) that has the following composition: [Pt $_{64.0}$ Ir $_{2.5}$ Rh $_{0.7}$ Os $_{0.1}$ Pd $_{0.1}$ Fe $_{30.2}$ Cu $_{1.9}$ Ni $_{0.4}$], corresponding to “(Pt, Ir)₂(Fe, Cu)” (anal. 10, Tables 5, 6).

The subhedral grain shown in Figure 2D is compositionally zoned, and consists of a Pt₃Fe-type alloy in the core [(Pt $_{3.04}$ Os $_{0.04}$ Rh $_{0.03}$ Ru $_{0.01}$) $_{\Sigma 3.12}$ (Fe $_{0.80}$ Cu $_{0.08}$) $_{\Sigma 0.88}$: anal. 15, Tables 1, 2], mantled by texturally heterogeneous Pt–Fe–Cu alloy(s). The latter are fine-grained, enriched in Cu, and range in composition from [(Pt $_{2.93}$ Os $_{0.03}$ Rh $_{0.04}$) $_{\Sigma 3.00}$ (Fe $_{0.80}$ Cu $_{0.19}$) $_{\Sigma 0.99}$: anal. 25, Tables 1, 2] to [(Pt $_{3.14}$ Os $_{0.03}$ Rh $_{0.03}$ Pd $_{0.02}$ Ru $_{0.02}$) $_{\Sigma 3.24}$ (Fe $_{0.64}$ Cu $_{0.11}$) $_{\Sigma 0.75}$: anal. 8, Tables 3, 4].

In all cases (Figs. 2A–D), a Pt₃Fe-type alloy(s) (isoferroplatinum or Fe-rich platinum) occurs in the core, which is poor in Cu (up to 2 at. %), and is mantled by Cu-enriched alloys, such as tetraferroplatinum [Pt $_{1+x}$ (Fe,Cu) $_{1-x}$ with 7.9–9.9 at. % Cu], Pt₃(Fe,Cu) with 4.7 at. % Cu, or tulameenite with 15.6–18.2 at. % Cu. Compositional zoning of this type is not uncommon in naturally occurring Pt–Fe–(Cu) alloys. For example, Tolstikh *et al.* (2000) reported a Pt–Fe alloy rimmed by a “Pt₃Cu”-type alloy in the Pustaya River placer deposit from the Koryak–Kamchatka belt of Alaskan-type intrusions, eastern Russia. Presumably, special conditions are required to stabilize a “Pt₃(Cu,Fe)”-type solid solution.

TABLE 8. ATOM PROPORTIONS IN Pt–Fe–(Cu) ALLOYS (*apfu*) WITH $0.9 < \Sigma$ PGE : (Fe+Cu+Ni) < 1.1 FROM PLACER DEPOSITS, BRITISH COLUMBIA

	Pt	Ir	Os	Rh	Pd	Ru	Fe	Cu	Ni	Σ PGE / (Fe+Cu+Ni)
1	49.20	0.52	0.13	0.52	0.04	0.00	24.65	15.64	9.30	1.02
2	49.47	0.00	0.00	0.45	0.15	0.00	22.96	18.15	8.83	1.00
3	48.16	3.45	0.00	1.51	0.14	0.00	38.40	7.99	0.36	1.14
4	47.42	3.69	0.07	1.36	0.22	0.11	38.78	7.94	0.41	1.12
5	49.52	0.00	0.06	0.35	0.03	0.00	27.62	21.21	1.21	1.00
6	46.20	4.28	0.13	1.15	0.18	0.03	33.00	14.63	0.41	1.08
7	48.60	0.67	0.21	0.47	0.00	0.00	22.58	26.22	1.25	1.00
8	47.98	0.00	0.27	0.39	0.00	0.00	21.45	29.08	0.83	0.95
9	47.91	0.00	0.15	0.27	0.07	0.00	25.35	24.94	1.31	0.94
10	46.91	3.19	0.07	0.29	0.18	0.00	24.65	21.73	2.98	1.03
11	48.49	0.00	0.00	0.36	0.06	0.00	24.94	17.46	8.70	0.96
12	49.12	1.88	0.36	0.95	0.10	0.11	37.15	9.93	0.40	1.11
13	50.14	1.21	0.06	1.04	0.36	0.00	41.94	3.91	1.36	1.12

Anal. 1 to 13: members of the tulameenite–tetraferroplatinum solid-solution series; the analytical results (in wt.%) are listed in Table 7.

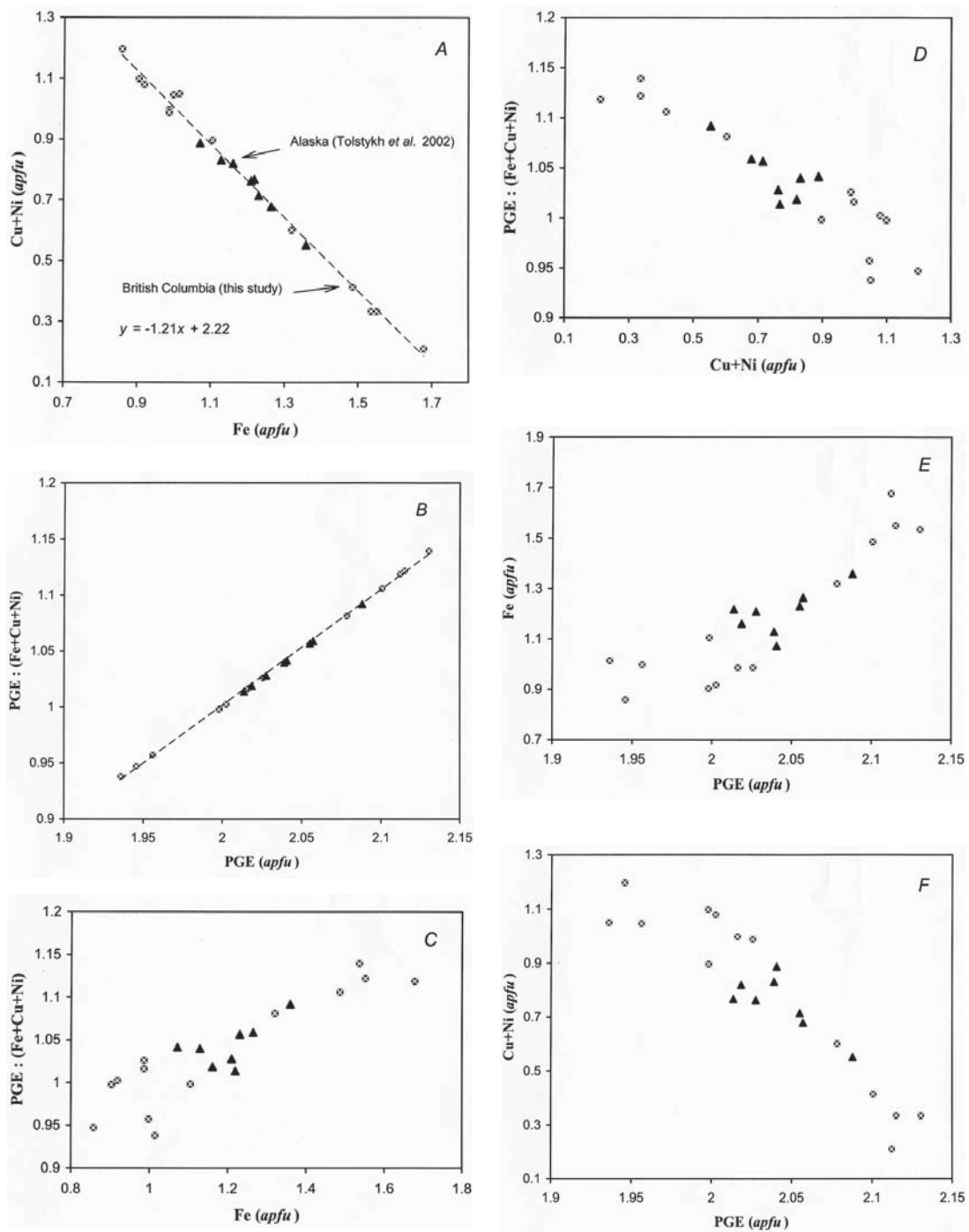


FIG. 8. Compositional variations of the tetraferroplatinum-tulameenite series observed in placer deposits from British Columbia (squares with inscribed crosses: this study) and from the Salmon River placer, Goodnews Bay, Alaska (triangles: Tolstykh *et al.* 2002) in terms of the plot of Fe versus Cu + Ni (A), of the atomic PGE:(Fe + Cu + Ni) ratio versus a total PGE content (B), versus Fe (C), and versus Cu + Ni (D), Fe versus PGE (E), and Cu + Ni versus PGE (F). The values are expressed in apfu ($\Sigma\text{atoms} = 4$).

This suggestion is consistent with the evidence for unmixing between Pt₃Cu and Pt₃Fe, which was reported from a placer derived from an Alaskan-type complex in eastern Madagascar (Augé & Legendre 1992).

Origin of the zoning in Pt–Fe–Cu alloys

There is a general similarity between the observed patterns of zoning (Figs. 2A–D) and those of zoned intermetallic compounds from the Noril'sk complex, Siberia, which consist of atokite–rustenburgite [(Pt,Pd)₃Sn] in the core mantled by Cu-rich stannides of the taimyrite–tatyanaite series (Barkov *et al.* 2000b). Therefore, A₃B-type cubic phases form the Cu-poor core in these zoned PGM intergrowths, which are mantled by the Cu-rich PGM. We infer that this zoning is likely primary in origin, and formed by fractional crystallization of original solid-solutions under closed-system conditions, as a result of increase in the activity of Cu species in the remaining liquid after an early-stage crystallization of the Cu-poor core(s). The Cu-rich Pt–Fe alloys were then deposited, after a significant decrease in temperature, around the core zone, or at their periphery, at a late or final stage of crystallization of the zoned alloys.

In summary, the textures (Figs. 2B,C) and compositions indicate the following sequence of crystallization: [Pt,Ir,Rh]₃Fe: “core” → [(Pt,Ir,Rh)_{1+x}(Fe,Cu)_{1-x}: “rim”] → [“(Pt,Ir)₂Fe”: narrow “outer rim”]. Our EMP data suggest that this “core” and the “outer rim” have approximately the same maximum content of Pt (64 at.%), which points to the existence of a genetic relationship between these zones. We thus infer that the Cu-rich “rim” deposited after the Cu-poor “core” as a result of decrease in temperature and increase in the activity of Cu. The “outer rim” [“(Pt,Ir)₂(Fe,Cu)”] could represent a residual liquid, a small volume of which may have remained after crystallization of the rim-like tetraferroplatinum zone (Figs. 2B, C). Alternatively, this “rim” may represent a reaction or alteration-induced feature, a possibility that is discussed below.

Reaction or alteration features: evidence for a late-stage Pt enrichment

A placer grain (~1 mm) with a “Pt₂Fe”-type bulk composition [Pt_{61.0}Ir_{2.8}Rh_{1.1}Pd_{0.2}Fe_{31.3}Cu_{3.14}Ni_{0.4}] exhibits a narrow zone (30–50 μm across), at the grain boundary of a Pt₃Fe-type alloy [Pt_{69.8}Ir_{2.1}Rh_{0.4}Fe_{27.4}Cu_{0.1}Ni_{0.1}], interpreted to be a reaction zone. The EMP data indicate that this zone is enriched in Pt and is somewhat poorer in Ir and Rh, and relatively poor in Fe, Cu, and Ni relative to the bulk grain. Possibly, this zone lost Fe as a result of high-temperature reaction or subsolidus re-equilibration between the “Pt₂Fe” alloy and a coexisting chromite or magnetite. However, the corresponding depletion in Cu and Ni cannot be explained by a reaction of this type. The EMP data indicate that the ΣPGE value is greater by 7.2 at.%, whereas (Fe + Cu +

Ni) is lower by 7.2 at.% in the reaction zone relative to the bulk grain. Thus, the Pt–Fe alloy may have locally reacted with a sulfide liquid or, alternatively, with a fluid phase during crystallization in a primary environment. Such reaction could have resulted in a partial removal of the base metals in the sulfide or fluid, and in the proportional increase in Pt, thus promoting the local formation of “Pt₃Fe” instead of “Pt₂Fe”. A general similarity exists between textures observed in this placer grain and in a tiny crystal of Pt–Fe–(Cu) alloys, which consists of a PtFe-type alloy in the core and a Pt₃Fe-type alloy in the rim, enclosed within chromite in the Tulameen complex (Nixon *et al.* 1990).

The characteristic texture of another grain of placer Pt–Fe alloys (Fig. 2E) also provides evidence for a Pt enrichment and removal of Fe late in the crystallization history or after crystallization. The original alloy is of a Pt₃(Fe,Cu)-type (unaltered and gray in Fig. 2E) and having the composition Pt 85.62, Ir 1.51, Os 1.86, Rh 1.40, Pd 0.38, Ru 0.25, Fe 5.08, Cu 1.92, Ni 0.11, a total 98.13 wt.%, which corresponds to [Pt_{73.2}Rh_{2.3}Os_{1.6}Ir_{1.3}Pd_{0.6}Ru_{0.4}Fe_{15.2}Cu_{5.0}Ni_{0.3}]. This alloy is rimmed and replaced by a veinlet-like alloy phase [*i.e.*, “alteration zones”, AZ, which are brighter in Fig. 2E] of the following composition: Pt 88.55, Ir 1.70, Os 1.84, Rh 1.41, Pd 0.29, Ru 0.21, Fe 1.85, Cu 1.96, Ni 0.04, a total 97.88 wt.%, or [Pt_{81.7}Rh_{2.4}Os_{1.8}Ir_{1.6}Pd_{0.5}Ru_{0.4}Fe_{6.0}Cu_{5.5}Ni_{0.1}]. These data indicate that the original alloy and the alloy developed in the AZ are distinct in their contents of Pt and Fe, whereas they are quite uniform in terms of contents of the other elements: Rh, Os, Ir, Pd, Ru, and Cu. In addition, the ΣPGE:(Fe + Cu + Ni) ratio of the latter alloy (AZ) is 7.6, which is much greater than that of the original alloy before alteration (3.9), or than the maximum value of this ratio (*ca.* 6) observed in all compositions of the analyzed grains of Pt–Fe alloy.

We suggest that these rim- and veinlet-like zones richer in Pt and poor in Fe (Fig. 2E) formed as a result of interaction of the original Pt–Fe alloy with a low-temperature fluid, leading to a selective removal of Fe and simultaneous addition of Pt. Thus, Fe and Pt were remobilized and redistributed in the scale of this alloy grain; in contrast, the other elements remained essentially immobile. The evidence for hydrothermal mobilization of Pt, Pd and Ni was reported in zoned Pd–Pt–Ni sulfides from the Penikat complex in Finland, for example (Barkov *et al.* 2004).

Interestingly, a certain degree of similarity may exist between the observed textures in the placer Pt–Fe alloy grains and textures of placer Au–Ag alloy, which consist of a Au-rich rim (poor in Ag), possibly formed under supergene conditions (*e.g.*, Knight *et al.* 1999a, and references therein). Such analogy would lead to an alternative, though less probable, hypothesis, implying that some of the Pt-rich and Fe-poor zones observed in the placer Pt–Fe–Cu alloy grains could have formed as a result of Fe removal in supergene processes.

Minor Ir, Rh, and Pd in various Pt–Fe–Cu alloys

Our EMP data on minor contents of Ir, Rh, and Pd in various Pt–Fe–Cu alloys [*i.e.*, Pt₃Fe-type alloys, Fe-rich Pt with the ΣPGE:(Fe + Cu + Ni) ratio of 3.6–5.6, members of the tetraferroplatinum–tulameenite series, and “Pt₂Fe”-type alloys] reveal that the data points generally plot along, or relatively near, the Ir–Rh and Rh–Pd joins. In contrast, no data points plot along the Pd–Ir join (Fig. 7). A compositional trend was previously reported for Pt₃Fe-type alloys from various localities, extending from the Ir corner toward the Rh corner and then to the Pd corner in the Pd–Ir–Rh diagram, and was interpreted to reflect a compositional change with decreasing temperature (Tolstikh *et al.* 2002, and references therein). In general, our data (Fig. 7) are consistent with these compositions, and imply the existence of Pd–Ir avoidance for the various Pt–Fe–Cu alloys, which are associated in the placer deposits examined.

TABLE 9. COMPOSITIONS OF VARIOUS Ir- AND Os-DOMINANT ALLOYS AND Ru-ENRICHED ALLOYS (wt.%) FROM Au–PGE PLACER DEPOSITS, BRITISH COLUMBIA

	Cu	Fe	Ni	Pt	Ir	Os	Pd	Rh	Ru	Total
12C 1	0.00	0.13	0.00	0.00	36.82	62.91	0.07	0.02	0.38	100.33
12C 2	0.00	0.30	0.08	5.40	59.96	31.88	0.00	0.51	1.94	100.07
12C 3	0.00	0.20	0.07	0.79	60.20	37.19	0.00	0.12	0.86	99.43
12C 4	0.02	0.58	0.05	14.96	61.71	19.45	0.00	1.14	2.10	100.01
12C 5	0.00	0.09	0.00	0.00	36.35	61.42	0.00	0.11	0.85	98.82
12C 6	0.00	0.21	0.02	0.00	43.09	56.53	0.06	0.00	0.86	100.77
12C 7	0.01	0.27	0.04	2.04	63.34	32.28	0.00	0.13	1.23	99.34
12C 8	0.00	1.09	0.13	3.53	85.93	5.47	0.00	0.87	1.75	98.77
12C 9	0.00	0.18	0.04	8.62	52.74	34.64	0.09	0.71	2.46	99.48
12C 10	0.00	0.36	0.09	3.97	67.42	26.19	0.00	0.16	0.68	98.87
12C 11	0.00	0.18	0.07	0.38	62.54	35.03	0.00	0.20	1.95	100.35
12C 12	0.00	0.31	0.03	0.00	67.33	31.21	0.00	0.05	1.00	99.93
16A 13	0.00	0.24	0.02	7.43	53.58	34.61	0.00	1.76	2.23	99.87
16A 14	0.00	0.24	0.05	0.49	40.56	53.96	0.00	0.37	2.93	98.60
40A 15	0.00	1.85	0.08	9.05	77.95	7.58	0.00	1.26	2.09	99.86
40A 16	0.00	0.07	0.05	3.77	37.37	39.49	0.00	0.77	17.85	99.37
40A 17	0.00	0.20	0.09	1.04	59.49	36.43	0.00	0.19	1.49	98.93
40A 18	0.00	0.20	0.08	1.01	61.83	36.28	0.00	0.21	1.68	101.29
40A 19	0.00	0.17	0.06	1.04	61.53	36.19	0.00	0.22	1.74	101.03
40A 20	0.01	0.34	0.10	7.26	53.10	32.77	0.00	1.18	4.57	99.33
40A 21	0.00	0.69	0.07	2.36	82.93	9.27	0.00	0.73	3.21	99.26
40A 22	0.00	0.17	0.02	0.89	40.21	49.65	0.05	0.73	7.63	99.35
40A 23	0.00	0.17	0.11	5.57	59.33	27.49	0.03	0.56	5.99	99.25
40A 24	0.00	0.00	0.00	0.84	0.00	99.64	0.14	0.14	0.00	100.76
40A 25	0.03	0.47	0.02	9.58	61.46	23.31	0.00	2.09	4.68	101.64
16A 26	0.02	0.06	0.00	1.73	2.97	93.85	0.03	0.58	1.17	100.41
16A 27	0.05	0.06	0.00	1.73	6.78	89.14	0.07	0.63	1.35	99.81
40A 28	0.01	1.63	0.08	8.07	77.03	10.19	0.00	2.00	1.79	100.80
40A 29	0.03	1.58	0.09	8.00	75.97	10.17	0.00	1.88	1.83	99.55
40A 30	0.00	0.11	0.04	1.38	36.60	55.37	0.00	0.58	5.30	99.38
40A 31	0.00	0.21	0.07	2.84	41.14	37.21	0.00	1.57	16.24	99.28
40A 32	0.00	0.25	0.04	2.86	40.80	36.91	0.00	1.57	16.11	98.54
40A 33	0.00	0.15	0.04	3.80	36.97	38.08	0.06	0.95	18.83	98.88

Anal. 15: an intergrowth with “(Pt, Ir), Fe”. Anal. 24: a subhedral lath (40 × 12 μm) enclosed by a Pt₃Fe grain. Anal. 25: 30 × 12–15 μm grain intergrown with tulameenite at the boundary of a “Pt₃Fe” grain. Anal. 26: 30 × 8 μm grain at the boundary of a Pt–Fe alloy grain. Anal. 27: 30 × 6 μm grain in intergrowth with amphibole, which are enclosed by a Fe-rich Pt grain. Anal. 28 and 29: crystallographically oriented exsolution-lamellae in a “Pt₃Fe” alloy host. 1–33: results of WDS analyses (JEOL–8600 electron microprobe); Co was not detected (<0.05 wt.%).

Ir- and Os-dominant alloys, and Ru-rich alloys

The EMP analyses of various Ir- and Os-dominant alloys and Ru-rich alloys (Tables 9, 10), which occur as individual grains or mutual intergrowths with Pt–Fe alloys, yielded the following mean composition and compositional ranges (in at.% for *n* = 23): Ir 53.20 (31.45–82.58), Os 33.56 (5.31–62.51), Ru 7.39 (0.71–30.47), Pt 3.41 (0.0–14.12), Rh 1.06 (0.0–3.16), Pd 0.03 (0.0–0.16), Fe 1.17 (0.2–5.92), and Ni 0.18 (0.0–0.42). Note that the compositions of exsolution lamellae or micro-inclusions of Ir–Os–Ru–(Pt) alloys are not included here. The predominance of Ir in the mean composition of the grains of Ir-, Os-, and Ru-rich alloys reflects the preponderance of Ir-dominant alloys (*ca.* 61% of the Ir–Os–Ru alloy grains). The overall compositional variations of Ir–Os–Ru–(Pt) alloys are shown in an Ir–Os–Ru diagram in Figure 9. The compositions of the majority of these alloy grains plot in the Ir field, outside the immiscibility region defined by Harris & Cabri (1991) and Cabri *et al.* (1996). Grain compositions form a broad array extending along the Ir–Os join, and Ru contents are generally minor (Fig. 9). Four of these alloy grains, however, are relatively enriched

TABLE 10. ATOM PROPORTIONS (*apfu*) OF THE Ir- AND Os-DOMINANT ALLOYS AND Ru-RICH ALLOYS FROM PLACER DEPOSITS, BRITISH COLUMBIA

	Cu	Fe	Ni	Pt	Ir	Os	Pd	Rh	Ru
1	0.00	0.43	0.00	0.00	36.20	62.51	0.12	0.04	0.71
2	0.00	0.99	0.26	5.15	57.98	31.15	0.00	0.91	3.56
3	0.00	0.69	0.22	0.77	59.41	37.09	0.00	0.21	1.61
4	0.05	1.92	0.15	14.12	59.10	18.82	0.00	2.03	3.82
5	0.00	0.30	0.00	0.00	36.15	61.74	0.00	0.20	1.61
6	0.00	0.71	0.06	0.00	41.93	55.60	0.10	0.00	1.60
7	0.02	0.91	0.13	1.98	62.32	32.10	0.00	0.23	2.31
8	0.00	3.61	0.42	3.34	82.58	5.31	0.00	1.55	3.19
9	0.00	0.60	0.12	8.23	51.13	33.94	0.16	1.29	4.53
10	0.00	1.24	0.28	3.88	66.79	26.22	0.00	0.30	1.29
11	0.00	0.61	0.24	0.36	60.56	34.28	0.00	0.36	3.60
12	0.00	1.04	0.11	0.00	65.98	30.91	0.00	0.10	1.87
13	0.00	0.80	0.05	7.02	51.37	33.53	0.00	3.16	4.07
14	0.00	0.79	0.15	0.47	39.45	53.04	0.00	0.67	5.42
15	0.00	5.92	0.25	8.30	72.52	7.13	0.00	2.18	3.70
16	0.00	0.20	0.14	3.18	32.00	34.18	0.00	1.22	29.07
17	0.00	0.67	0.29	1.01	58.62	36.28	0.00	0.34	2.79
18	0.00	0.66	0.25	0.95	59.45	35.25	0.00	0.37	3.07
19	0.00	0.55	0.20	0.99	59.37	35.29	0.00	0.40	3.20
20	0.03	1.12	0.31	6.76	50.18	31.30	0.00	2.09	8.21
21	0.00	2.26	0.23	2.22	79.20	8.95	0.00	1.31	5.83
22	0.00	0.54	0.05	0.81	37.28	46.52	0.09	1.27	13.45
23	0.00	0.54	0.34	5.18	55.96	26.20	0.05	0.99	10.74
24	0.00	0.02	0.00	0.81	0.00	98.67	0.25	0.25	0.00
25	0.08	1.48	0.07	8.66	56.37	21.60	0.00	3.59	8.16
26	0.06	0.21	0.00	1.65	2.87	91.94	0.05	1.06	2.15
27	0.16	0.19	0.00	1.66	6.60	87.64	0.13	1.14	2.49
28	0.04	5.18	0.25	7.34	71.10	9.51	0.00	3.44	3.14
29	0.09	5.08	0.28	7.37	71.02	9.61	0.00	3.29	3.26
30	0.00	0.37	0.14	1.29	34.65	52.98	0.00	1.03	9.54
31	0.00	0.61	0.19	2.40	35.38	32.34	0.00	2.52	26.56
32	0.00	0.75	0.11	2.44	35.33	32.30	0.00	2.54	26.53
33	0.00	0.43	0.12	3.19	31.45	32.74	0.09	1.50	30.47

The analytical results (in wt.%) are listed in Table 9.

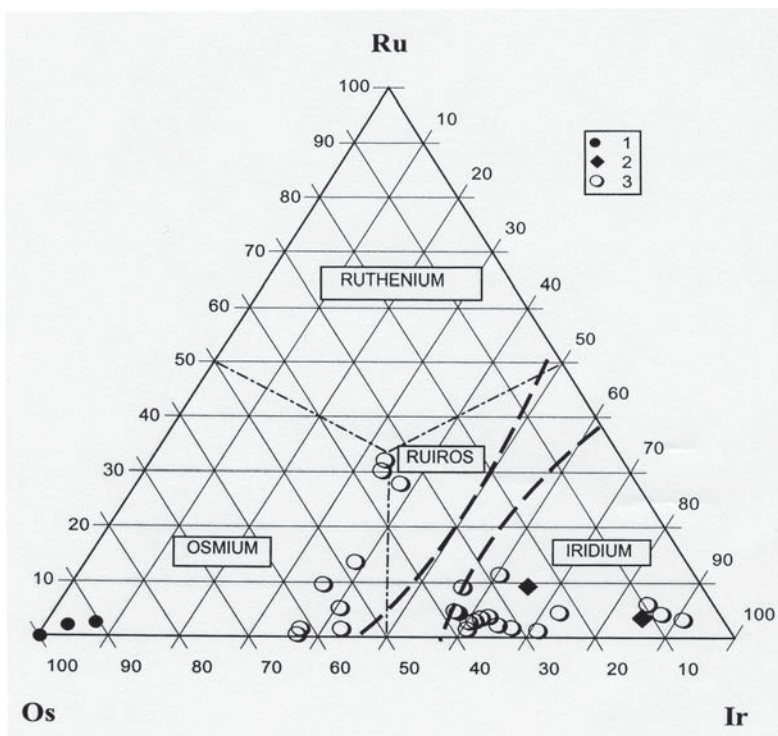


FIG. 9. Compositions of Ir- and Os-dominant alloys from the placer deposits examined in British Columbia, plotted in the Os–Ir–Ru diagram (in at.%). The dashed lines show the miscibility gap of Harris & Cabri (1991) and Cabri *et al.* (1996). Filled circles (1) are micro-inclusions or lamellae of Os-dominant alloys enclosed by Pt–Fe alloys. Filled diamonds (2) are micro-inclusions or lamellae of Ir-dominant alloys enclosed by Pt–Fe alloys. Open circles (3) are individual placer grains of Ir–Os-rich alloys or their mutual intergrowths with Pt–Fe alloys. One of these grains corresponds compositionally to rutheniridosmine, and compositions of the other two grains are plotted close to the border of the compositional field of rutheniridosmine (RUIROS).

in Ru (16.1–18.8 wt.% Ru or 26.5–30.5 at.% Ru), and their atomic Ir:Os:Ru proportion is close to 1:1:1 (anal. 16, 31–33, Tables 9, 10). These Ru-rich compositions plot near the border of the rutheniridosmine field and one of these alloys has Ir > Os > Ru, consistent with a rutheniridosmine composition (Fig. 9).

The compositions of fine exsolution lamellae of Ir-dominant alloys in Pt–Fe alloys plot in the same compositional field as the Ir–(Os)-rich alloy placer grains. In contrast, the Os-rich exsolution phases are distinct and characterized by an extreme enrichment in Os (Figs. 9, 10).

Nickel-rich cuproiridsite [(Cu,Ni,Fe)(Ir,Rh,Pt)₂S₄]

Results of EMP analyses (Table 11) indicate that a complex PGE and base-metal sulfide, which occurs as oriented lamellae in a Pt₃Fe-type alloy (Fig. 2F), is a thiospinel (AB₂X₄). This is the second reported

occurrence of PGE thiospinel in Canada. Previously, Corriveau & Laflamme (1990) described occurrences of various PGE thiospinels from ophiolites at Thetford Mines, Quebec.

The family of PGE thiospinels includes cuprorhodsite, cuproiridsite [CuRh₂S₄ and CuIr₂S₄; Rudashevsky *et al.* 1985], malanite [Cu(Pt,Ir,Rh)₂S₄; Yu 1996], and ferrorhodsite [(Fe,Cu)(Rh,Pt,Ir)₂S₄; Rudashevsky *et al.* 1998], which all have a spinel-type structure and display considerable mutual solid-solutions. Barkov & Fleet (2004) argued that a miscibility gap likely exists close to “CuPt₂S₄” in the system CuRh₂S₄–CuIr₂S₄–“CuPt₂S₄”. The analyzed thiospinel (anal. 1, Table 11) is unusually enriched in Ni and compositionally corresponds to nickel-rich cuproiridsite–(cuprorhodsite–malanite). It is likely related to synthetic NiIr₂S₄ (*e.g.*, Berlincourt *et al.* 1981) and to Cu_{1-x}Ni_xRh₂S₄ (Hart *et al.* 2000).

The PGE thiospinels are commonly associated with various Alaskan-type complexes, though they may also

occur in ophiolitic chromitites (Corrivaux & Laflamme 1990, Augé & Maurizot 1995), in podiform chromitites in orogenic lherzolite complexes (Garuti *et al.*

TABLE 11. ELECTRON-MICROPROBE DATA ON NICKEL-RICH CUPROIRIDSITE, COOPERITE, FERROUS SULFURIAN SPERRYLITE AND A PLATARSITE-LIKE PHASE FROM PLACERS, BRITISH COLUMBIA

No.	Cu	Fe	Ni	Pt	Ir	Rh	Pd	Co	S	As	Total
40A 1	7.10	1.31	2.94	13.47	40.88	8.86	n.d.	0.03	25.42	n.d.	100.0
16A 2	n.d.	n.d.	n.d.	82.48	n.d.	n.d.	0.62	n.d.	16.91	n.d.	100.0
16A 3	n.d.	1.16	0.02	55.03	n.d.	4.19	0.22	0.13	1.93	37.47	100.15
91B 4	n.d.	0.26	0.25	69.11	n.d.	0.22	1.57	n.d.	12.37	17.38	101.31

No.	Cu	Fe	Ni	Σ	Ir	Rh	Pt	Pd	Co	Σ	S	As	S+As
1	0.58	0.12	0.26	0.97	1.11	0.45	0.36	-	<0.01	1.92	4.12	-	4.12
2	-	-	-	-	-	0.88	0.01	-	0.90	1.10	-	-	1.10
3	-	0.07	<0.01	-	0.13	0.93	<0.01	<0.01	1.15	0.20	1.65	1.85	1.85
4	-	0.01	0.01	-	0.01	1.06	0.04	-	1.13	1.16	0.70	1.86	1.86

Anal. 1: cuproiridsite, anal. 2: cooperite, anal. 3: sperrylite-like phase, and 4: platarsite-like phase (results of WDS analyses: JEOL-8600 electron microprobe). The atom proportions are based on a total of 7 atoms per formula unit, *apfu* (anal. 1), 2 *apfu* (anal. 2), and 3 *apfu* (anal. 3). n.d.: not detected. Os and Ru were sought, but not detected. The total in anal. 4 includes 0.15 wt.% Sb.

1995), and in layered intrusions (Barkov *et al.* 2000a). Although most of these thiospinels are commonly poor in Ni, their Ni-dominant (unnamed) analogues likely exist, as is implied by synthetic NiIr₂S₄ (Berlincourt *et al.* 1981) or by nickel-rich cuprorhodsite (0.44 *apfu* Ni) from the Baimka placer deposit, which is associated with Alaskan-type complexes, northeastern Russia (Gornostayev *et al.* 1999). The observed Fe content of the analyzed cuproiridsite is relatively high (0.12 *apfu*: Table 11), and points to the presence of the ferrorhodsite component. PGE thiospinels rich in Fe have been reported from the Penikat layered complex, Finland, where Fe is incorporated via a coupled substitution mechanism of the type: [^AFe³⁺ + 2 ^BRh³⁺ + ^ACu⁺ + 2 ^BPt⁴⁺ (+ 2 Ir⁴⁺)] (Barkov *et al.* 2000a).

A metal-rich ferrous rhodian sulfurian sperrylite [(Pt,Rh,Fe)(As,S)_{2-x}]

An unusual sulfarsenide of Pt (anal. 3, Table 11), containing appreciable Rh (4.2 wt.%), Fe (1.2 wt.%), and S (1.9 wt.%), occurs as blocky and interlaced lamellar grains at the boundary of a Pt₃Fe-type alloy grain, and as abundant veinlets within this placer grain

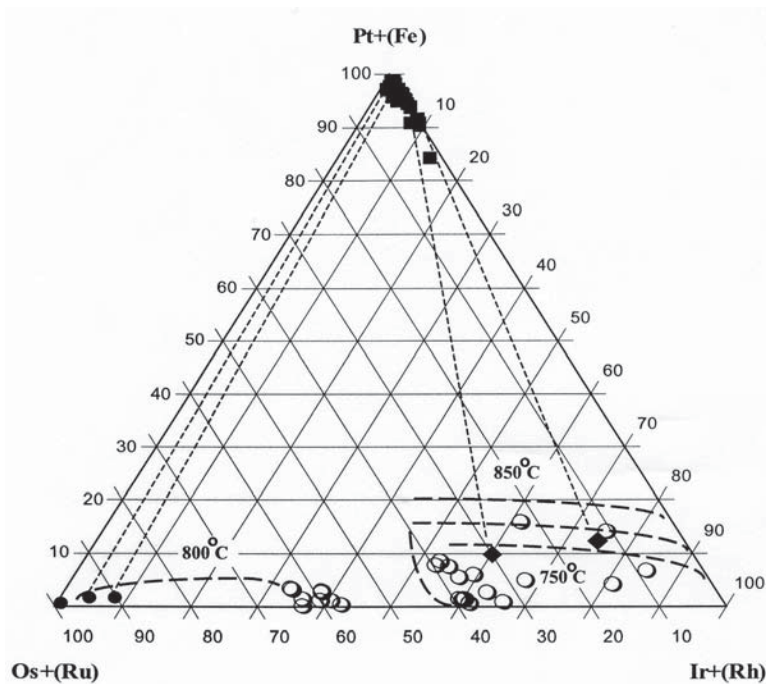


FIG. 10. Pseudoternary phase-diagram for the Os + (Ru) - Pt + (Fe) - Ir + (Rh) system [slightly modified from Slansky *et al.* (1991), and references therein], showing estimated temperatures of equilibration for the exsolution lamellae or micro-inclusions of Os-dominant (filled circles) and Ir-dominant (filled diamonds) alloys, exsolved from Pt-Fe alloys (filled squares).

(Figs. 3B, C). An EMP analysis yields a sperrylite-type formula $[(\text{Pt}_{0.93}\text{Rh}_{0.13}\text{Fe}_{0.07})_{\Sigma 1.15}(\text{As}_{1.65}\text{S}_{0.20})_{\Sigma 1.85}]$. The atomic (Rh + Fe):S ratio is 1.0, and indicates that Rh and Fe may be incorporated as a sulfarsenide component (“hollingworthite–arsenopyrite”) according to the following scheme: $[(\text{Rh} + \text{Fe})^{3+} + (\text{AsS})^{3-} = \text{Pt}^{2+} + (\text{As}_2)^{2-}]$. This is consistent with reaction mechanisms previously formulated for the sperrylite–hollingworthite (RhAsS) series (Barkov & Fleet 2004), which has been reported from the Nomgon complex, Mongolia (Izokh & Mayorova 1990). Barkov *et al.* (2004) suggested that Fe occurs as the arsenopyrite component in a zoned grain of irarsite (IrAsS)–hollingworthite from the Penikat layered complex, and that the incorporation of Fe is governed there by the following mechanism of substitution: $[(\text{Rh} + \text{Fe})^{3+} = \text{Ir}^{3+}]$. Note that Rh and Fe are closely associated in this substitution; the association of these elements is also implied by the composition of the sperrylite-type phase from British Columbia. Rhodian sulfurian sperrylite was previously reported from the Imandra complex in Russia, implying a limited solid-solution toward the pyrite-type $\text{Rh}_{1-x}\text{S}_2$ (i.e., “ Rh_2S_5 ” or $\text{Rh}_{0.8}\text{S}_2$): $[0.4 \text{Rh}^{3+} + 0.4 \text{Rh}^{2+} + 0.2 \text{Me}^{\square} + (\text{S}_2)^{2-} = \text{Pt}^{2+} + (\text{As}_2)^{2-}$; Barkov & Fleet 2004].

On the other hand, the (As + S) value of the presently analyzed sperrylite-type phase is relatively low (1.85 *apfu*; anal. 3, Table 11), which may imply the presence of vacancies at the As site. Thus, an alternative substitution-scheme may be proposed, which assumes limited incorporation of Rh and Fe in the form of a monosulfide phase, (Rh,Fe)S, possibly related to the (Rh,Fe,Ni)S described from Ethiopia (Cabri *et al.* 1996). Natural solid-solutions between mono- and dichalcogenides are uncommon, though possible (especially for NiAs-type derivative structures), as indicated, for example, by the existence of an extensive solid-solution series between the Pd–Ni mono- and ditellurides (Barkov *et al.* 2002).

*Platarsite-type phase [PtAs_{1-x}S_{1+x}]
or unnamed Pt(S,As)_{2-x}*

This phase is highly unusual; it forms a narrow rim (ca. 5 μm across) around a Pt₃Fe-type placer grain [(Pt_{2.85}Pd_{0.25}Rh_{0.05}Os_{0.02}Ir_{0.01}Ru_{0.01}) $\Sigma 3.19$ (Fe_{0.72}Cu_{0.09}Ni_{0.01}) $\Sigma 0.82$; sample no. VLE–2001–91B; Fig. 1]. Its formula is $(\text{Pt}_{1.06}\text{Pd}_{0.04}\text{Rh}_{0.01}\text{Fe}_{0.01}\text{Ni}_{0.01})_{\Sigma 1.13}\text{S}_{1.16}\text{As}_{0.70}\text{Sb}_{<0.01}$, with the *Me*:(As + S) atomic proportions virtually identical to those of the ferrous rhodian sulfurian sperrylite (anal. 3, 4, Table 11). This phase may be related to platarsite, PtAsS (Cabri *et al.* 1977, Szymański 1979, Cabri & Laflamme 1981). Barkov & Fleet (2004) suggested that the incorporation of Me^{3+} (Rh, Ir or Ni) in platarsite, which is probably a mixed-valence compound $[\text{Pt}^{4+}_{0.5}\text{Pt}^{2+}_{0.5}[\text{AsS}]^{3-}]$, is governed by the $[2\text{Me}^{3+} = (\text{Pt}^{4+} + \text{Pt}^{2+})]$ substitution. On the other hand, the analyzed phase from British Columbia has the S-dominant composition, which contrasts with

As-excess compositions of platarsite and platarsite-type compounds (e.g., Cabri & Laflamme 1981, Barkov & Fleet 2004). This phase may thus represent a new (unnamed) species having the following formula: $(\text{Pt,Pd,Rh})(\text{S,As})_{2-x}$. A more detailed characterization of this phase is impossible because of its minute grain-size.

Cooperite [PtS] and unnamed (Ir,Rh,Pt)S (?)

Cooperite occurs as a partial rim around a Pt₃Fe-type alloy grain (Fig. 4C). Platinum and S are its main constituents, and Pd is minor (0.6 wt.%); all the other elements were found to be below the limit of detection (anal. 2, Table 11).

Fragments of an Ir–Rh–(Pt) sulfide, likely relics of a single broken grain, are preserved at the margin of a Pt₃Fe-type alloy (Figs. 4D, E). Only preliminary and semiquantitative compositional data could be obtained owing to the minute grain-size (<5 μm). However, the estimated atomic proportions differ from those of kashinite [(Ir,Rh)₂S₃], and, instead, seem consistent with the (Ir,Rh,Pt)S-type formula $[(\text{Ir}_{0.45}\text{Rh}_{0.37}\text{Pt}_{0.08})_{\Sigma 0.9}\text{S}_{1.1} : \Sigma \text{atoms} = 2; \text{Cu, Fe, Ni, Co, Os, Ru, Pd, and As were not detected}]$. If this suggestion is correct, a possible relationship with “IrS” is implied (cf. Berlincourt *et al.* 1981). The “IrS” phase has been first synthesized by heating “IrS₃” (Ir_{1-x}S₂) or IrS₂ in N₂ at 700°C (Wöhler *et al.* 1933). Biltz *et al.* (1937) did not confirm the presence of “IrS”, however. The other reported phases with similar atomic proportions are [(Ir_{0.56}Rh_{0.25}Ni_{0.15}Pt_{0.03}) $\Sigma 1.0$ S_{1.0}] from China (Yu *et al.* 1974), (Rh,Pd)S from Borneo, Malaysia, and (Rh,Ir,Fe,Ni)S from Yubdo, Ethiopia (Cabri *et al.* 1996).

Implications from silicate micro-inclusions in PGM

The EMP data for silicate inclusions in various PGE alloy grains are given in Table 12 [diopside: anal. 1, Fig. 3D; augite: anal. 2; amphiboles: anal. 3, 4; talc: anal. 5, and clinocllore: anal. 6; which show high values of *mg#*, i.e., 100 $\text{Mg}/(\text{Mg} + \text{Fe})$, where all Fe is FeO]. The lower analytical totals in some cases reflect grain sizes less than the excitation volume of the electron beam. An inclusion of euhedral quartz (Figs. 3F, 4F, anal. 7, Table 12) is enclosed in the Ir-dominant alloy $[\text{Ir}_{59.10}\text{Os}_{18.82}\text{Pt}_{14.12}\text{Ru}_{3.82}\text{Rh}_{2.03}\text{Fe}_{1.92}\text{Ni}_{0.15}]$. Compositionally, the amphiboles are ferro-edenite (anal. 3), which is intergrown with diopside (Fig. 3D), and a potassian sodic-calcic amphibole like richterite (anal. 4) intergrown with native Os (Fig. 4B). These high-Mg amphiboles are generally devoid of Cl, consistent with the Mg–Cl avoidance principle. However, the potassian richterite grain contains minor Cl (0.4 wt.%; Table 12) whose incorporation into the amphibole structure was likely promoted by its K-rich composition (cf. Oberti *et al.* 1993). The high *mg#* values of these ferromagnesian silicates (Table 12) suggest that they formed in a

relatively magnesian primary environment, although the *mg#* values may also reflect subsolidus re-equilibration or high-temperature reaction. Interestingly, the composition of diopside [$\text{Ca}_{51}\text{Mg}_{40}\text{Fe}_9$; sample 40a; anal. 1, Table 12)], enclosed by a composite grain of Ir–Os–(Pt) and Pt–(Ir)–Fe alloys (Fig. 3D) is nearly identical to [$\text{Ca}_{50}\text{Mg}_{40}\text{Fe}_{10}$] reported from “inclusion no. 5” in a Pt–Fe nugget associated with the Tulameen Alaskan-type complex, British Columbia (*cf.* Table 12 in Nixon *et al.* 1990). This correspondence and the sample location, which is relatively near the Tulameen complex (Fig. 1), suggest a similar igneous source for these placer PGE alloys. The presence of euhedral quartz enclosed within the Ir–Os alloy (sample no. 12c, Fig. 4F), which probably crystallized from a trapped intercumulus liquid, is consistent with a mafic source, probably a mineralized pyroxenite from the Atlin area

(Fig. 1), and is not consistent with dunite or another rock containing olivine.

Associations of the placer PGM

Most of the placer samples examined in this study (Fig. 1) are characterized by a preponderance of Pt–Fe–(Cu) alloys and, to a lesser degree, Ir-dominant alloys. In contrast, the Ir-dominant alloys are the principal PGM in sample no. 12c (Table 13), collected in the Atlin area (Fig. 1). The crystal faces preserved on many of the PGM grains examined (*e.g.*, Figs. 2A, B, D, 3A, D, E) provide evidence for a relatively short distance of their transport from lode sources.

The Pt–Fe–(Cu) alloys constitute the majority of the PGM grains present in the concentrates (Table 13). Pt₃Fe-type alloys are well known in various Alaskan-type and ophiolite complexes. They may be also present in mineralized rocks of other types, even some “exotic” PGE-bearing rocks such as kimberlite (Stone & Fleet 1990). In general, the placer alloys analyzed in this study are relatively enriched in Cu and Rh, and are notably depleted in Ru (Tables 1, 2). These characteristics are representative of Pt–Fe alloys from Uralian–Alaskan-type complexes (*e.g.*, Rudashevsky & Zhdanov 1983, Cabri *et al.* 1996), with few exceptions

TABLE 12. ELECTRON-MICROPROBE DATA ON INCLUSIONS OF SILICATE MINERALS IN Pt–Fe AND Ir–Os ALLOYS, BRITISH COLUMBIA

No.	<i>Di</i> 1	<i>Aug</i> 2	<i>Amp</i> 3	<i>Amp</i> 4	<i>Tlc</i> 5	<i>Chl</i> 6	<i>Qtz</i> 7
SiO ₂ , wt.%	53.40	54.15	40.47	55.02	62.99	28.81	98.29
TiO ₂	0.09	0.14	0.23	1.01	0.01	0.23	n.d.
Al ₂ O ₃	1.59	1.67	10.48	19.50	0.03	15.86	1.00
Cr ₂ O ₃	n.d.	0.04	0.05	0.03	0.03	0.02	n.d.
FeO	5.76	8.75	15.60	4.53	1.56	16.01	n.d.
MnO	0.12	0.29	0.12	0.12	n.d.	0.27	n.d.
MgO	13.79	16.70	8.40	2.61	30.84	19.17	n.d.
NiO	0.05	n.d.	0.04	n.d.	0.35	0.14	n.d.
CaO	24.60	13.90	10.48	6.68	0.01	0.26	n.d.
Na ₂ O	0.57	0.30	3.50	1.71	0.03	0.01	n.d.
K ₂ O	0.01	0.10	0.53	5.09	n.d.	0.05	n.d.
Cl	n.d.	n.d.	n.d.	0.43	n.d.	0.06	n.d.
F	n.d.	n.d.	n.d.	n.d.	n.d.	n.d.	n.d.
O ²⁺ Cl	-	-	-	0.10	-	0.01	-
Total	99.98	96.04	89.90	96.63	95.85	80.88	99.29
O	6	6	23	23	11	14	2
<i>Si apfu</i>	1.98	2.04	6.62	7.61	3.99	3.13	0.99
Ti	<0.01	<0.01	0.03	0.11	<0.01	0.02	-
Al	0.07	0.07	2.02	3.18	<0.01	2.03	0.01
Cr	-	<0.01	<0.01	<0.01	<0.01	<0.01	-
Fe	0.18	0.28	2.14	0.52	0.08	1.46	-
Mn	<0.01	0.01	0.02	0.01	-	0.02	-
Mg	0.76	0.94	2.05	0.54	2.91	3.11	-
Ni	<0.01	-	<0.01	-	0.02	0.01	-
Ca	0.98	0.56	1.84	0.99	<0.01	0.03	-
Na	0.04	0.02	1.11	0.46	<0.01	<0.01	-
K	<0.01	<0.01	0.11	0.90	-	<0.01	-
Cl	-	-	-	0.10	-	0.01	-
<i>mg#</i>	81.0	77.3	49.0	50.7	97.3	68.1	-
Ca	50.9	31.6	-	-	-	-	-
Mg	39.7	52.9	-	-	-	-	-
Fe	9.3	15.5	-	-	-	-	-

Columns 1 and 3: a 40- μm intergrowth of diopside (*Di*) and amphibole (*Amp*), enclosed by a composite grain of Ir–Os–(Pt) and “(Pt, Ir), Fe” alloys (sample 40A). Column 2: a relic of augite (*Aug*; *ca.* 20 \times 10 μm) at the boundary of Fe-rich platinum (sample 16A). Column 4: amphibole (*Amp*; *ca.* 30 μm) intergrown with a lath of native Os, enclosed by Fe-rich platinum (sample 16A). Column 5: a 30- μm inclusion of talc (*Tlc*) in a Pt₃Fe-type alloy (sample 40A). Column 6: a 40- μm grain of clinocllore (*Chl*) at the boundary of Fe-rich platinum (sample 16A). Column 7: a euhedral grain of quartz (*Qtz*; *ca.* 60 μm) enclosed by an Ir–Os–(Pt) alloy (sample 12C). 1 to 7: results of WDS analyses (JEOL-8600 microprobe). n.d. not detected. *mg#* = 100 Mg / (Mg + Fe).

TABLE 13. A LISTING OF PGM SPECIES AND PGE-RICH PHASES, AND THEIR RELATIVE ABUNDANCES IN THE SAMPLES EXAMINED FROM Au–PGM PLACERS IN BRITISH COLUMBIA

Mineral or phase	VLE 2001 -95a	VLE 2001 -40a	VLE 2001 -93	VLE 2001 -16a	VLE 2001 -12c
Fe-rich platinum [†]	0	0	1	3	1
6 < Σ PGE / (Fe+Cu+Ni) < 5					
Fe-rich platinum [†]	0	1	2	7	0
5 < Σ PGE / (Fe+Cu+Ni) < 4					
Pt ₃ Fe-type alloys	2	9	0	11	4
“Pt, Fe”-type alloys	3	8	0	0	0
Tetraferroplatinum– tulameenite series	2	4	0	0	1
Iridium [Ir-dominant Ir–Os–(Pt) alloys]	0	4	0	1	9
Osmium [Os-dominant Os–Ir–(Pt) alloys]	0	0	0	1	3
Rutheniridosmine [*]	0	4	0	0	0
Cuproiridosite [‡]	0	1	0	0	0
Cooperite [‡]	0	0	0	1	0
Sperrylite-type phase [§] [(Pt,Rh,Fe)(As,S) ₂]	0	0	0	1	0
Unnamed (Ir,Rh,Pt)S (3) [§]	0	1	0	0	0

Note: The sample location and terrane affinities for these samples (no. 95a, 40a, 93, 16a, and 12c) are shown in Figure 1. The numbers of PGM grains listed here include single placer grains and various PGM and PGE-rich phases that occur in composite grains or mutual intergrowths, except for micro-inclusions and exsolution lamellae of Ir- and Os-dominant alloys in Pt–Fe–(Cu) alloy grains.

* Rutheniridosmine and related Ru-rich alloys of Ir and Os, which are close to rutheniridosmine in composition (Fig. 9).

† These PGM and PGE-rich phases occur in trace or minor amounts; they formed at a late stage of crystallization (see text for discussion). In addition, a platarrsite-like phase [PtAs_{1–2}S_{1–2} or Pt(S,As)₂] was observed (sample #91B; Fig. 1) as a narrow rim around a grain of Pt₃Fe-type alloy.

‡ According to IMA rules, the species formerly referred to as ferroan platinum is now to be called Fe-rich platinum (Bayliss *et al.* 2005).

(*e.g.*, Augé & Maurizot 1995). The atomic proportions of minor Rh, Ir, and Pd in the placer grains (Fig. 7) are rather similar to those reported in Pt₃Fe-type alloys from Alaska. In addition, the Pt–Fe alloys (Fig. 10) exhibit an enrichment in Ir + (Rh) relative to Os + (Ru), and extend toward Ir + (Rh), similar to patterns reported from Alaska (*cf.* Tolstykh *et al.* 2002). Following observations of Rudashevsky & Zhdanov (1983), the presence of elevated Ir (up to 13.4 wt.%: Table 1) could possibly imply the derivation from an Alaskan–(Uralian–Aldan)-type chromitite. Low contents of Cr in the associated silicates and hydrous silicates (Table 12) could imply crystallization from trapped residual liquids depleted in Cr, which is thus consistent with a chromite-rich source. The characteristic association between Pt and Ir, inferred from the mineralogical data, is consistent with an Alaskan-type source, as is also the low-S character of the primary environment (*cf.* Naldrett & Cabri 1976), which is evident from the virtual absence of base-metal sulfides in intergrowth with the PGE-rich alloys, and from the presence of traces of PGE sulfides in these placer grains. The observed Pt–Ir association is consistent with results of experiments on S-bearing systems, which provide evidence of PGE fractionation between alloy and sulfide liquid according to atomic weights rather than melting points of the PGE (Fleet & Stone 1991).

Some other compositional and textural characteristics of the placer PGM are also consistent with derivation from an Alaskan-type complex. Such features include (Figs. 2 to 4): the characteristic rims of members of the tetraferroplatinum–tulameenite series or of Pt₃(Fe,Cu) around Fe-rich platinum – isoferroplatinum, the late-stage Pt–(Rh–Fe) sulfarsenide, and oriented exsolution-lamellae of Ir- and Os-rich alloys or Ni-rich cuproiridsite (*cf.* Nixon *et al.* 1990, Cabri *et al.* 1996, Johan *et al.* 2000, Tolstykh *et al.* 2000, 2002, Garuti *et al.* 2002, Malitch & Thalhammer 2002). We also note that the “Pt₂Fe”-type alloys were only observed in the placer samples collected in the vicinity of the Tulameen complex (Fig. 1, Table 13), which is thus the likely primary source for these PGM, in agreement with the derivation of related “Pt_{2.5}(Fe,Ni,Cu)_{1.5}” alloys from the Tulameen complex (Nixon *et al.* 1990).

Is the presence of rutheniridosmine consistent with an Alaskan-type source?

Rutheniridosmine and other Ru-rich alloys of Os and Ir are typically, but not necessarily, associated with ophiolite-type complexes. A few grains of alloy analyzed in this study display high contents of Ru (up to 26.5–30.5 at.%: anal. 16, 31–33, Table 10, Fig. 9), and rutheniridosmine is present in one sample (no. 40a: Table 13). Nevertheless, these observations do not necessarily exclude an Alaskan-type source. An abundance of Os–Ir–Ru–Pt alloys (typically Os-dominant), which are rich in Ru, and associated with

subordinate Pt–Fe alloys rather than rutheniridosmine, may conclusively point to an ophiolitic source (*e.g.*, Weiser & Bachmann 1999). The presence of rutheniridosmine has been also reported in association with Alaskan-type complexes, *e.g.*, in a placer associated with the Tulameen complex (Harris & Cabri 1973, and Table 9 in Nixon *et al.* 1990), which is likely the case for the analyzed rutheniridosmine (sample no. 40a; Fig. 1) in the Durance River alluvium, France (Johan *et al.* 1990), and from Nizhnii Tagil, the Urals (*e.g.*, Cabri *et al.* 1996).

We suggest that the high contents of Ru observed in rutheniridosmine and related Os–Ir–(Ru) alloys in association with rutheniridosmine (Fig. 9) may reflect a low level of sulfur fugacity in the system. At sulfur fugacities below the Ru–RuS₂ buffer, Ru may be readily incorporated in the Ir–Os–Ru alloy phase, instead of as common disulfides of the laurite–erlichmanite series [RuS₂–OsS₂], which have been not observed in the PGM placer concentrates studied herein.

Potential primary sources for the placer PGM

Two different primary sources may be suggested for the analyzed placer PGM (Table 13). Our mineralogical data are consistent with the Alaskan-type source for most of the PGM examined in samples no. 95a, 40a, and 93. The observed association of these placer samples with the island-arc terranes of Quesnellia, which are the recognized host for a suite of Alaskan-type intrusions (Fig. 1), also implies the derivation from Alaskan-type complexes. In contrast, sample no. 12c is closely associated with an ophiolitic (oceanic) terrane in the Atlin area (Fig. 1); besides, this sample is notably distinct from the other examined samples in the strong preponderance of the Ir- and Os-dominant alloys relative to the Pt–Fe–(Cu) alloys (Table 13). Thus, the Atlin ultramafic-mafic intrusions, which are potential sources for PGM-bearing placers in the Atlin area (Cabri *et al.* 1996), may represent the source rocks for the associated PGM in sample 12c. However, compositions of the Ir- and Os-dominant alloys analyzed in this sample are relatively poor in Ru (<2.5 wt.%, Table 9), and an additional investigation is thus required to confirm the proposed ophiolite origin for these placer PGM. Similar to sample 12c is placer sample 16a, spatially associated with an ophiolite terrane in the Cache Creek area (Fig. 1); on the other hand, an Alaskan-type complex is situated nearby (Fig. 1). Thus, this or a related Alaskan-type intrusion could presumably be the source for the placer PGM present in this sample (principally Pt–Fe alloys: Table 13). In addition, a relative enrichment in Cu and Rh and depletion in Ru, observed in Pt–Fe alloys from samples 16a and 12c (Tables 1, 2), are consistent rather with the Alaskan-type source. It cannot therefore be excluded that the placer PGM present in these two samples were in fact derived from both of these potential sources, Alaskan-type and ophiolitic.

Crystallization history of the associated PGM

A high-temperature origin of the associated Pt–Fe alloys and Ir–Os alloys, and a similar temperature of their crystallization, are implied by the observed exsolution of Ir–(Os)-rich alloy from the host Pt–Fe alloy (Fig. 3A), and, *vice versa*, by the exsolution of Pt–Fe alloy from the Ir-rich alloy (Fig. 3D). We note the following points.

(1) Most of the observed PGM species and varieties, such as the Cu-rich Pt–Fe alloys [tetraferroplatinum–tulameenite and $\text{Pt}_3(\text{Fe,Cu})$], cooperite, Ni-rich cuproiridsite, Pt-rich sulfarsenides [(Pt,Rh,Fe)(As,S) $_{2-x}$ and Pt(S,As) $_{2-x}$], and “(Ir,Rh,Pt)S”, are only present in minor or trace quantities and in intimate association with Pt–Fe alloy grains, not with Ir–Os-rich alloys, and their speciation and compositions are likely related to the crystallization of the coexisting Pt–Fe alloys.

(2) Apparently, these minor PGM formed at an advanced or late stage of magmatic (or postmagmatic) crystallization, after the coexisting (host) Pt–Fe alloys, as is indicated by their textural characteristics: the presence of rims and rim-like grains (Figs. 2A, B, 3B, 4C), veinlets (Fig. 3C), micrograins at the boundary of Pt–Fe alloy(s) (Figs. 4D, E), and of “crystallographically” oriented lamellae (Fig. 2F).

(3) The fine exsolution-induced domains of Ir-dominant alloy (Fig. 3A) and of native Os (Fig. 4A), which display intergrowth relationships with the “potassic richterite” (Fig. 4B) and occur at the Pt–Fe alloy grain boundary, in common with micrograins of Ir–Os alloys, also imply crystallization at a lower temperature, which was controlled to a large degree by the crystallization of the coexisting (host) Pt–Fe alloy(s).

(4) A high temperature of crystallization of a Pt_3Fe -type alloy would clearly promote the incorporation of elevated levels of Ir, in accordance with the experimental data of Makovicky & Karup-Møller (2000), who observed that, in the system Pt–Ir–Fe–S, the solubility of Ir in synthetic Pt_3Fe decreases with decreasing temperature (29.3 at.% Ir at 1100°C, and 23.6 at.% Ir at 1000°C). Thus, a normal drop in temperature, associated with cooling, and corresponding decrease in the solubility of Ir could likely produce the exsolution lamellae or micro-inclusions of Ir–(Os)-rich alloys, which are “crystallographically” oriented and are enclosed within the host Pt–Fe alloy(s). The compositions of Os- and Ir-dominant alloys, which exsolved from the coexisting Pt–Fe alloys, imply uniform temperatures of equilibration of approximately 750 to 800°C (Fig. 10).

(5) The Cu-rich Pt–Fe alloys observed in the “rim-like zones” of zoned intergrowths appear to have formed as a result of a drop in temperature and increase in the activity of Cu in the remaining liquid after an early crystallization of the Cu-poor Pt–Fe alloys (*i.e.*, the “core zones”: Figs. 2A, B, D). The observed similarity with the zoned intergrowths of Pt–Pd–(Cu) stannides

from the Noril’sk complex is noteworthy (*cf.* Barkov *et al.* 2000b).

(6) The Cu-poor Pt–Fe alloys likely crystallized under conditions of a low sulfur fugacity in a magmatic environment poor in overall S. Presumably, levels of sulfur fugacity have increased with progressive crystallization of these alloys, thus promoting the local formation of the Ni-rich cuproiridsite by exsolution (Fig. 2F), of the rim-like grains of late-stage Ir–Rh–Pt sulfide (Fig. 4E), cooperite (Fig. 4C) and of the Pt–Rh–(Fe) sulfarsenides (*e.g.*, Fig. 3B). Similar to S, As must have been an incompatible component during the crystallization of the Pt–Fe alloy. Relative levels of As must have increased at a late stage of crystallization, when the lamellar and rim-like grains of this sulfarsenide (*e.g.*, Fig. 3C) precipitated from a late-stage fluid.

ACKNOWLEDGEMENTS

The first author expresses his sincere gratitude and appreciation to Professor Michael E. Fleet. This study was made possible with financial support from the British Columbia Geological Survey and the Natural Sciences and Engineering Research Council of Canada, which is gratefully acknowledged. Menghua Liu of the A.D. Edgar Laboratory, University of Western Ontario, London, Ontario, is thanked for his technical assistance with the EMP analyses. V.M.L. is grateful to the following individuals for providing information, access to placer mining properties and samples of concentrate: Peter Burjoski, Mike Swenson, Ken Herron, Dale and Debora Harrison, and John English. Dave Mate and Travis Ferbey assisted with field work, data analysis and figure preparation. We thank Louis J. Cabri and Yuanming Pan for constructive criticism on this contribution.

REFERENCES

- AUGÉ, T. & LEGENDRE, O. (1992): Platinum–iron nuggets from alluvial deposits in eastern Madagascar. *Can. Mineral.* **30**, 983–1004.
- _____ & MAURIZOT, P. (1995): Stratiform and alluvial platinum mineralization in the New Caledonia ophiolite complex. *Can. Mineral.* **33**, 1023–1045.
- BARKOV, A.Y. & FLEET, M.E. (2004): An unusual association of hydrothermal platinum-group minerals from the Imandra layered complex, Kola Peninsula, northwestern Russia. *Can. Mineral.* **42**, 455–467.
- _____, _____, MARTIN, R.F. & ALAPIETI, T.T. (2004): Zoned sulfides and sulfarsenides of the platinum-group elements from the Penikat layered complex, Finland. *Can. Mineral.* **42**, 515–537.
- _____, LAFLAMME, J.H.G., CABRI, L.J. & MARTIN, R.F. (2002): Platinum-group minerals from the Wellgreen

- Cu–Ni–PGE deposit, Yukon, Canada. *Can. Mineral.* **40**, 651–669.
- _____, MARTIN, R.F., HALKOAHO, T.A.A. & POIRIER, G. (2000a): The mechanism of charge compensation in Cu–Fe–PGE thiospinels from the Penikat layered intrusion, Finland. *Am. Mineral.* **85**, 694–697.
- _____, _____, POIRIER, G. & YAKOVLEV, Y.N. (2000b): The taimyrite–tatyanaite series and zoning in intermetallic compounds of Pt, Pd, Cu, and Sn from Noril'sk, Siberia, Russia. *Can. Mineral.* **38**, 599–609.
- BAYLISS, P., KAESZ, H.D. & NICKEL, E.H. (2005): The use of chemical-element adjectival modifiers in mineral nomenclature. *Can. Mineral.* **43**, 1429–1433.
- BERLINCOURT, L.E., HUMMEL, H.H. & SKINNER, B.J. (1981): Phases and phase relations of the platinum-group elements. In *Platinum-Group Elements: Mineralogy, Geology, Recovery* (L.J. Cabri, ed.). *Can. Inst. Mining, Metall., Petroleum, Spec. Vol.* **23**, 19–45.
- BILTZ, W., LAAR, J., EHRLICH, P. & MEISEL, K. (1937): The systematic study of affinity. LXXIV. The sulfides of iridium. *Z. anorg. allgem. Chem.* **233**, 257–281.
- BOWLES, J.F.W. (1990): Platinum–iron alloys, their structural and magnetic characteristics in relation to hydrothermal and low-temperature genesis. *Mineral. Petrol.* **43**, 37–47.
- CABRI, L.J. & FEATHER, C.E. (1975): Platinum–iron alloys. Nomenclature based on a study of natural and synthetic alloys. *Can. Mineral.* **13**, 117–126.
- _____, & GENKIN, A.D. (1991): Re-examination of platinum alloys from lode and placer deposits, Urals. *Can. Mineral.* **29**, 419–425.
- _____, HARRIS, D.C. & WEISER, T.W. (1996): Mineralogy and distribution of platinum-group mineral (PGM) placer deposits of the world. *Explor. Mining Geol.* **5**, 73–167.
- _____, & LAFLAMME, J.H.G. (1981): Analyses of minerals containing platinum-group elements. In *Platinum-Group Elements: Mineralogy, Geology, Recovery* (L.J. Cabri, ed.). *Can. Inst. Mining Metall., Petroleum, Spec. Vol.* **23**, 151–173.
- _____, _____ & STEWART, J.M. (1977): Platinum-group minerals from Onverwacht. II. Platarsite, a new sulfarsenide of platinum. *Can. Mineral.* **15**, 385–388.
- _____, OWENS, D.R. & LAFLAMME, J.H.G. (1973): Tulameenite, a new platinum–iron–copper mineral from placers in the Tulameen River area, British Columbia. *Can. Mineral.* **12**, 21–25.
- _____, ROSENZWEIG, A. & PINCH, W.W. (1977): Platinum-group minerals from Onverwacht. I. Pt–Fe–Cu–Ni alloys. *Can. Mineral.* **15**, 380–384.
- CORRIVAUX, L. & LAFLAMME, J.H.G. (1990): Minéralogie des éléments du groupe du platine dans les chromitites de l'ophiolite de Thetford Mines, Québec. *Can. Mineral.* **28**, 579–595.
- FLEET, M.E. & STONE, W.E. (1991): Partitioning of platinum-group elements in the Fe–Ni–S system and their fractionation in nature. *Geochim. Cosmochim. Acta* **55**, 245–253.
- GARUTI, G., GAZZOTTI, M. & TORRES-RUIZ, J. (1995): Iridium, rhodium, and platinum sulfides in chromitites from the ultramafic massifs of Finero, Italy, and Ojen, Spain. *Can. Mineral.* **33**, 509–520.
- _____, PUSHKAREV, E.V. & ZACCARINI, F. (2002): Composition and paragenesis of Pt alloys from chromitites of the Uralian–Alaskan-type Kytlym and Uktus complexes, northern and central Urals, Russia. *Can. Mineral.* **40**, 1127–1146.
- GORNOSTAYEV, S.S., CROCKET, J.H., MOCHALOV, A.G. & LAJOKI, K.V.O. (1999): The platinum-group minerals of the Baimka placer deposits, Aluchin horst, Russian Far East. *Can. Mineral.* **37**, 1117–1129.
- HARRIS, D.C. & CABRI, L.J. (1973): The nomenclature of the natural alloys of osmium, iridium and ruthenium based on new compositional data of alloys from world-wide occurrences. *Can. Mineral.* **12**, 104–112.
- _____, & _____ (1991): Nomenclature of platinum-group-element alloys: review and revision. *Can. Mineral.* **29**, 231–237.
- HART, G.L.W., PICKETT, W.E., KURMAEV, E.Z., HARTMANN, D., NEUMANN, M., MOEWES, A., EDERER, D.L., ENDOH, R., TANIGUCHI, K. & NAGATA, S. (2000): Electronic structure of $\text{Cu}_{1-x}\text{Ni}_x\text{Rh}_2\text{S}_4$ and CuRh_2Se_4 : band-structure calculations, X-ray photoemission, and fluorescence measurements. *Phys. Rev. B: Condens. Matter Mater. Phys.* **61**, 4230–4237.
- IZOKH, A.E. & MAYOROVA, O.N. (1990): A rhodium-bearing sperrylite from the Nomgon complex (Mongolia). *Dokl. Akad. Nauk SSSR* **313**, 1212–1215 (in Russ.).
- JOHAN, Z., OHNENSTETTER, M., FISCHER, W. & AMOSSÉ, J. (1990): Platinum-group minerals from the Durance River alluvium, France. *Mineral. Petrol.* **42**, 287–306.
- _____, _____, SLANSKY, E., BARRON, L.M. & SUPPEL, D. (1989): Platinum mineralization in the Alaskan-type intrusive complexes near Fifield, New South Wales, Australia. 1. Platinum-group minerals in clinopyroxenites of the Kelvin Grove prospect, Owendale intrusion. *Mineral. Petrol.* **40**, 289–309.
- _____, SLANSKY, E. & KELLY, D. (2000): Platinum nuggets from the Kompam area, Enga Province, Papua New Guinea: evidence for an Alaskan-type complex. *Mineral. Petrol.* **68**, 159–176.
- KNIGHT, J.B., MORISON, S.R. & MORTENSEN, J.K. (1999a): The relationship between placer gold particle shape, rimming, and distance of fluvial transport as exemplified by gold from the Klondike District, Yukon Territory, Canada. *Econ. Geol.* **94**, 635–648.

- _____, MORTENSEN, J.K. & MORISON, S.R. (1999b): Lode and placer gold composition in the Klondike District, Yukon Territory, Canada: implications for the nature and genesis of Klondike placer and lode gold deposits. *Econ. Geol.* **94**, 649-664.
- LEVSON, V.M. & GILES, T.R. (1993): Geology of Tertiary and Quaternary gold-bearing placers in the Cariboo Region, British Columbia. *British Columbia Ministry of Energy and Mines, Bull.* **89**.
- _____, MATE, D. & FERBEY, T. (2002): Platinum-group-element (PGE) placer deposits in British Columbia: characterization and implications for PGE potential. *In Geological Fieldwork 2001. British Columbia Geological Survey, Pap.* **2002-1**, 303-312.
- _____ & MORISON, S. (1995): Geology of placer deposits in glaciated environments. *In Past Glacial Environments – Sediments, Forms and Techniques* (J. Menzies, ed.). Pergamon Press, Oxford, U.K. (441-478).
- MAKOVICKY, E. & KARUP-MØLLER, S. (2000): Phase relations in the metal-rich portions of the phase system Pt–Ir–Fe–S at 1000°C and 1100°C. *Mineral. Mag.* **64**, 1047-1056.
- MALITCH, K.N. & THALHAMMER, O.A.R. (2002): Pt–Fe nuggets derived from clinopyroxenite–dunite massifs, Russia: a structural, compositional and osmium-isotope study. *Can. Mineral.* **40**, 395-418.
- NALDRETT, A.J. & CABRI, L.J. (1976): Ultramafic and related mafic rocks: their classification and genesis with special reference to the concentration of nickel sulfides and platinum-group elements. *Econ. Geol.* **71**, 1131-1158.
- NIXON, G.T., CABRI, L.J. & LAFLAMME, J.H.G. (1990): Platinum-group-element mineralization in lode and placer deposits associated with the Tulameen Alaskan-type complex, British Columbia. *Can. Mineral.* **28**, 503-535.
- OBERTHÜR, T., WEISER, T.W., GAST, L., SCHOENBERG, R. & DAVIS, D.W. (2002): Platinum-group minerals and other detrital components in the Karoo-age Somabula gravels, Gweru, Zimbabwe. *Can. Mineral.* **40**, 435-456.
- OBERTI, R., UNGARETTI, L., CANNILLO, E. & HAWTHORNE, F.C. (1993): The mechanism of Cl incorporation in amphibole. *Am. Mineral.* **78**, 746-752.
- RAICEVIC, D. & CABRI, L.J. (1976): Mineralogy and concentration of Au- and Pt-bearing placers from the Tulameen River area in British Columbia. *Can. Inst. Mining Metall., Bull.* **69**(770), 111-119.
- RUDASHEVSKY, N.S., MEN'SHIKOV, YU.P., MOCHALOV, A.G., TRUBKIN, N.V., SHUMSKAYA, N.I. & ZHDANOV, V.V. (1985): Cuprorhodsite CuRh_2S_4 and cuproiridsite CuIr_2S_4 – new natural thiospinels of platinum-group elements. *Zap. Vses. Mineral. Obshchest.* **114**, 187-195 (in Russ.).
- _____, MOCHALOV, A.G., MEN'SHIKOV, YU.P. & SHUMSKAYA, N.I. (1983): Ferronickelplatinum Pt_2FeNi – a new mineral species. *Zap. Vses. Mineral. Obshchest.* **112**, 487-494 (in Russ.).
- _____, _____ & _____ (1998): Ferro-rhodsite $(\text{Fe,Cu})(\text{Rh,Pt,Ir})_2\text{S}_4$ – a new mineral. *Zap. Vses. Mineral. Obshchest.* **127**(5), 37-41 (in Russ.).
- _____ & ZHDANOV, V.V. (1983): Accessory platinum mineralization of a mafic-ultramafic intrusion in Kamchatka. *Bull. Moscow Obshchest. Ispyt. Prirody, Otd. Geol.* **58**, 49-59 (in Russ.).
- SLANSKY, E., JOHAN, Z., OHNENSTETTER, M., BARRON, L.M. & SUPPEL, D. (1991): Platinum mineralization in the Alaskan-type intrusive complexes near Fifield, N.S.W., Australia. 2. Platinum-group minerals in placer deposits at Fifield. *Mineral. Petrol.* **43**, 161-180.
- STONE, W.E. & FLEET, M.E. (1990): Platinum–iron alloy (Pt_3Fe) in kimberlite from Fayette County, Pennsylvania. *Am. Mineral.* **75**, 881-885.
- SZYMAŃSKI, J.T. (1979): The crystal structure of platarsite, $\text{Pt}(\text{As}_2\text{S}_2)_2$, and a comparison with sperrylite, PtAs_2 . *Can. Mineral.* **17**, 117-123.
- TOLSTYKH, N.D., FOLEY, J.Y., SIDOROV, E.G. & LAAJOKI, K.V.O. (2002): Composition of the platinum-group minerals in the Salmon River placer deposit, Goodnews Bay, Alaska. *Can. Mineral.* **40**, 463-471.
- _____, SIDOROV, E.G., LAAJOKI, K.V.O., KRIVENKO, A.P. & PODLIPSKIY, M. (2000): The association of platinum-group minerals in placers of the Pustaya River, Kamchatka, Russia. *Can. Mineral.* **38**, 1251-1264.
- WEISER, T.W. & BACHMANN, H.-G. (1999): Platinum-group minerals from the Aikora river area, Papua New Guinea. *Can. Mineral.* **37**, 1131-1145.
- WÖHLER, L., EWALD, K. & KRALL, H. (1933): The sulfides, selenides and tellurides of the six platinum metals. *G. Ber.* **66B**, 1638-1652.
- YU, T.-H., LIN, S.-J., CHAO, P., FANG, C.-S. & HUANG, C.-S. (1974): A preliminary study of some new minerals of the platinum-group and another associated new one in platinum-bearing intrusions in a region in China. *Acta Geol. Sinica* **2**, 202-218 (in Chinese).
- YU, ZUXIANG (1995): Chengdeite – an ordered natural iron–iridium alloy. *Dizhi Xuebao* **69**, 215-220 (in Chinese).
- _____ (1996): New data on the cupric platinum (Pt^{3+}) and iridium (Ir^{3+}) sulfide – malanite. *Dizhi Xuebao* **70**, 309-314 (in Chinese).
- ZHERNOVSKY, I.V., MOCHALOV, A.G. & RUDASHEVSKY, N.S. (1985): Phase inhomogeneity of isoferroplatinum enriched in iron. *Dokl. Akad. Nauk SSSR* **283**, 196-200 (in Russ.).

Received August 30, 2004, revised manuscript accepted June 15, 2005.

APPENDIX: DESCRIPTIONS OF SAMPLE SITES OF THE PLACER CONCENTRATES*Sample VLE 2001-12c*

The concentrate sample was derived from the lower few meters of a paleochannel gravel deposit that overlies bedrock and underlies approximately 20 m of glacial sediments. The paleochannel deposits are strongly oxidized and, although mostly buried, they locally outcrop along the sides of the O'Donnell River valley. The overburden sequence consists of a capping diamicton underlain by crudely stratified gravels and several meters of horizontally bedded silts and sands. These deposits are interpreted, respectively, as till, proximal glaciofluvial gravels and glaciolacustrine sediments. The paleochannel gravels consist mainly of large-scale trough cross-bedded sands and pebble gravels with some cobble to boulder gravel beds up to about a meter thick. Sample 2001-12c was a heavy-mineral concentrate processed from the lower few meters of the unit and the upper half-meter of the bedrock.

Sample VLE 2001-16a

The site was not visited, but the following description is summarized from information provided by the miner. Mined materials occur on a low terrace about 25 m wide and one to six meters deep, with very little overburden (usually less than one meter). The gravels are horizontally stratified and subrounded to well rounded. Clasts are mainly in the pebble size-range, with up to about 40% cobbles and boulders. Clast lithologies, in order of abundance, include granitic rocks, schist, shale, quartz, limestone, and ultramafic rocks (serpentinite and jade). The local bedrock is highly altered shale and limestone with numerous quartz veins. Recovered gold is coarse (mainly >5 mm diameter), with rounded edges.

Sample VLE 2001-40a

The sample was collected at a small open-pit mine exploiting an alluvial fan placer. The placer gravels sit directly on bedrock and are one to two meters thick. They probably represent fluvial and colluvial sediments deposited prior to, and in the early stages

of, fan development. They are overlain by three to four meters of bouldery fan gravels with relatively low concentrations of placer minerals. The mined gravels are clast-supported, matrix-filled, large pebble to large cobble gravels with a muddy sand matrix. The gravels are mainly subangular and local in origin, although subrounded erratic boulders also are present. Cobble clusters and thin pebble gravel beds also occur. Gold nuggets are mostly flattened with rounded edges. They become more angular and coarser upstream. Reported gangue minerals include abundant magnetite, minor pyrite and rare garnet. The overburden sequence consists mainly of massive to crudely stratified, matrix-to clast-supported, cobble to boulder gravels. The clasts are subrounded, and erratic lithologies are common. The sequence is interpreted as an alluvial fan deposit consisting mainly of reworked glacial sediments.

Sample VLE 2001-93

The sample was derived from surface fluvial gravels overlying bedrock on a low terrace a few meters above river level. The geology of the site and detailed descriptions of the placer deposits are provided by Levson & Giles (1993). Holocene terrace gravels in the region generally overlie older, probably Tertiary, cemented gravels. Clasts are rounded to well rounded, and the gravels are well stratified. Gold grains are typically small (less than 1 mm) and flat with rounded edges. Reported gangue minerals include garnet, magnetite, pyrite and copper.

Sample VLE 2001-95a

The sample was derived from the upper meter of a modern river bar overlying bedrock, downstream of a steep, narrow channel. The gravels are variably rounded, sandy, and mainly in the pebble to cobble size-range. They are commonly iron-stained and poorly stratified. River gravels in the area are typically one to two meters deep and locally overlain by fine sands and muds. Reported gangue minerals include magnetite, copper minerals, garnet, and chromite. Gold grains up to about 0.25 g and platinum grains to 0.1 g are reported.